Chapter 3

Reconstructing atmospheric trace gas records from firn and ice core measurements

3.1 Introduction

Measurements of the air trapped in bubbles in polar ice are one of the main ways used to reconstruct changes in the composition of the atmosphere in the past. To do this, however, one needs to know how the ice core measurements relate to past atmospheric levels, which requires an understanding of the processes involved in storing the air in the ice. These processes may affect the age and composition of the air that eventually becomes enclosed in the ice. The ice originally falls as snow, and over a number of years becomes compacted, eventually trapping air into bubbles. The top (roughly) 70 m of this compacted snow, which is called *firn*, is porous and has open channels along which diffusion occurs. The air in the channels is in contact with the atmosphere, and changes in atmospheric composition diffuse very slowly through the firn column. Air at the bottom of the firn is gradually trapped into bubbles, as depicted in Figure 3.1.

In this chapter, a one-dimensional, finite difference model is developed to quantify the affects of firn diffusion and bubble trapping. The model and many of the calculations from this chapter are also described in Trudinger et al. (1997). The model is calibrated and tested using measurements of a range of different trace gases from the firn at DE08-2. It is then used to investigate the Law Dome CO_2 and $\delta^{13}CO_2$ ice core record, and firn records of $\delta^{13}CO_2$ from three different sites. An important application of the model is to determine the *isotopic diffusion correction*, which is required for measurements of $\delta^{13}C$

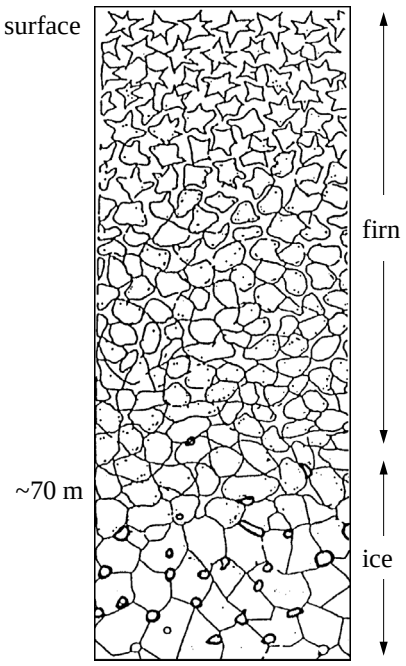

Figure 3.1: Representation of bubble close-off in firn, reproduced from Raynaud (1993).

in the firn and ice. The model is also used for dating firn samples, and to investigate how changes in the atmospheric growth rate of a species can alter the age of trapped air relative to the age of the host ice, which complicates the reconstruction of features in an ice core record. The main interest in this chapter is in reconstructing records of CO_2 and $\delta^{13}CO_2$ from firn and ice, however a number of other trace gases and isotopic ratios (CH_4, SF_6, $\Delta^{14}CO_2$, $\delta^{15}N_2$, $\delta^{13}CH_4$) are also studied to help give better insight into the firn processes.

3.2 Description of firn processes

The composition of the air stored in ice relative to the composition in the atmosphere is influenced mainly by two processes: gas diffusion through the firn and the progressive trapping of bubbles during the transition from firn to impermeable ice. Trapped air is younger than the surrounding ice because it is isolated from the atmosphere at the bottom of the firn (Berner et al., 1978; Schwander and Stauffer, 1984). Atmospheric

concentrations are also smoothed in time due to the gradual bubble close-off (Delmas et al., 1980; Schwander and Stauffer, 1984). The time span over which the trapping occurs depends mostly on the snow accumulation rate and can vary from several years at high accumulation rate sites, to hundreds of years at very low accumulation rate sites. For some time it was assumed that the firn layer was well mixed, and that air trapped in bubbles had essentially the same composition as that of the atmosphere at the time of bubble close-off (Schwander and Stauffer, 1984). However Schwander et al. (1988) pointed out that the firn is not well mixed, and that a delay of 5 years or longer is expected for gas diffusion through the firn. This slow mixing causes smoothing of atmospheric concentration variations at the close-off depth, while at the same time the slow mixing around the close-off region reduces the smoothing due to trapping. Consideration of the diffusion is most relevant for high accumulation rate sites, where the trapping time is comparable to the delay due to mixing.

Schwander et al. (1988) developed a one-dimensional model of diffusive gas transport in firn to quantify these processes. They measured the diffusivity of firn samples from Siple Station, Antarctica, for use in the model. Schwander et al. (1993) collected air from a number of depths through the firn at Summit in Greenland. The firn air samples were measured for a range of trace gases and isotopes, and the measurements were used to test the validity of the diffusion model. As measurements of firn air can cover the same period as direct measurements of some trace gases, they provide an excellent way to understand the firn processes, leading to better dating and interpretation of ice core measurements.

Firn air is also important for reconstructing atmospheric concentrations that may otherwise be unknown. Air is pumped out of the firn *in situ*, allowing much greater volumes of air to be collected than could be obtained by extracting air from bubbles trapped in ice, which currently requires the ice to be taken from the drilling site back to a laboratory. Measurement of some trace gases requires large amounts of air, for example $\delta^{13}CH_4$ currently requires up to 5 standard litres of air for a single measurement (Etheridge et al., 1998). This would translate to 50 kg of ice to give enough air for just one measurement. There are also some species that are believed to be affected by the trapping process, so measurements of trapped air cannot reliably give atmospheric levels. The O_2/N_2 ratio is an example of this, for reasons that will be explained shortly. Firn air

can also be used to confirm ice core measurements, as well as to link ice core measurements to modern records. At some sites, air at the bottom of the firn can be up to around 100 years old (Battle et al., 1996). Severinghaus et al. (1997) investigated the possibility of using sand dunes as archives of past air. Interpreting these measurements is very similar to using firn air, as in both cases an atmospheric signal diffuses through a porous media. Severinghaus et al. (1997) concluded that sand dunes may be useful for relatively inert trace gases with large atmospheric changes such as CFCs, but that microbial metabolism and fractionation of gases due to water vapour preclude their use for many other gases of interest (e.g. CO_2, N_2O, CH_4 and O_2).

There are a number of processes that impact the composition of air in the firn and ice, many of which are associated with the diffusion and trapping. Firstly, as gravity acts on different species according to their mass, it causes an enrichment of heavier species relative to lighter ones through the firn. This fractionation due to gravity has a large effect on isotopic ratios, as well as a moderate effect on trace gas mixing ratios, and measurements in the firn and ice need to be corrected to remove the effect. Gravitational fractionation will be discussed in more detail in Section 3.5.2. It is also believed that fractionation occurs during bubble trapping, as some species (for example, O_2) are partially excluded from the bubbles at close-off when channels of molecular size form (Craig et al., 1988; Bender et al., 1995; Battle et al., 1996). The excluded species diffuse up through the firn, altering the composition in the firn. Although this fractionation may occur for a number of species, O_2 is the most notable example. O_2 escapes more readily than N_2, and as anthropogenic changes in the O_2/N_2 ratio are proportionally very small, O_2/N_2 measurements from ice cores are believed to be unreliable.

Fractionation due to thermal diffusion can occur when there is a temperature gradient in the firn, such as due to seasonal temperature variations at the surface or abrupt changes in climate (Severinghaus and Sowers, 1995; Severinghaus et al., 1998). Thermal diffusion causes heavier species to become enriched in colder parts of the firn. In fact, signals caused by this fractionation were used by Severinghaus et al. (1998) to estimate the timing of the warming at the end of the Younger Dryas. At some sites, such as Vostok (Bender et al., 1994), there is mixing of the upper part of the firn, due perhaps to either convection or advection (wind pumping). This will have an important effect on the composition of

air in the firn, and will be particularly difficult to account for if the extent of the mixing varies considerably with time. Melt layers are another complication, and can occur when the snow at the surface partially melts. A melt layer can affect the air composition in two ways: first, by reducing the diffusive mixing and second, by introducing additional chemistry (Neftel et al., 1983). Sites with melt layers are generally avoided because of these complications, except for some recent measurements on Law Dome in the 1997-98 summer which targeted a heavy melt layer site (POINSETT) in the hope of finding air stored between summer melt layers in the firn, therefore with greatly reduced smoothing (D. M. Etheridge, pers. comm., 1998). *In situ* production of radioactive isotopes (e.g. $^{14}CO_2$, ^{14}CO) has been detected (Smith et al., 2000). The production occurs in the ice by cosmic ray induced spallation reactions on oxygen nuclei and the isotopes may migrate into the air in the bubbles, possibly by diffusion out of the ice lattice (V. A. Levchenko, pers. comm., 1999). This work may have important implications for the possible influence of CO_2 derived from impurities in the ice lattice on the measurements of CO_2 and its isotopes in ice core air.

3.3 The firn diffusion model

A 1-D, finite difference model of firn diffusion and trapping which is quite similar to that developed by J. Schwander (Schwander et al., 1988; 1993) will be used to quantify the firn processes. Ice sheet properties (density, open porosity, and diffusivity) are specified inputs to the model and are used to determine the diffusion in the open pore space and the gradual close-off of air into bubbles. The characteristics of the firn and ice are expressed in terms of several basic parameters and functions. The depth below the surface, z, of a particular layer of ice or firn increases with time as new snow accumulates at the surface. The model therefore uses a coordinate system that moves downward with respect to the surface, following the ice. The density, ρ, increases with depth from a surface value, ρ_0, of around 340 kg m^{-3} to the density of ice, ρ_i, which is about 918 kg m^{-3}. The snow accumulation rate, A, is expressed in terms of the mass per unit area per unit time (kg m^{-2} yr^{-1}) and is taken to be constant with time for each site. Temperature is assumed to be constant with depth, with different values used for each site. The seasonal variation of surface temperature measured at DE08 is about $\pm$10 K about the mean. This variation

will have a negligible effect on the diffusion coefficient compared with the variation due to other factors (mainly porosity) and is therefore not modelled.

The model uses mass coordinates, μ, defined by

$$\mu(z) \ = \int_0^z \rho(z')\, dz' \tag{3.1}$$

Density (or, more precisely, inverse density) is given in terms of the mass coordinates in the following form, which allows for seasonal variation in the density:

$$\rho(\mu)^{-1} = V(\mu) + \sigma(t, \mu)\, a(\mu) \tag{3.2}$$

where $V(\mu)$ is the deseasonalised value of the inverse density, $a(\mu)$ determines the amplitude of variations about $V(\mu)$ (the case with no such variability in ice properties corresponds to $a(\mu) \equiv 0$), and $\sigma(\mu, t)$ is a phase function that defines how much of the allowed variability for that level is actually exhibited. The important characteristic is that a fixed value of σ moves with each particular ice layer. The normal usage would be to have $-1 \leq \sigma \leq 1$. The simplest form of seasonal variation is to have $\sigma = \sin(2\pi t_{\text{precip}})$, where t_{precip} is the time in years at which the snow precipitated.

The model works with externally prescribed specifications of $V(\mu)$, $a(\mu)$, and $\sigma(\mu, t_0)$ at equally spaced values of μ. Since the accumulation rate is taken as constant at each site, the equally spaced mass coordinates, μ, are equivalent to equal increments in the age of the ice. In theory, as the accumulation rate and density profile are known, it is possible to calculate the depths of the mass coordinates, $z(\mu)$. However, in practice, because of variations in the annual accumulation rate and, more importantly, possible divergent or convergent flow of the ice at depth, the calculated $z(\mu)$ can vary somewhat from observations of depth versus the age of the ice. Where measurements are available, $z(\mu)$ will be specified to ensure that the model output is consistent with observations when it is given as a function of either depth or ice age. In the model the prescribed density is used to derive the ice properties that control diffusion and bubble trapping, while the depth is used for model output and for the layer thickness, $\Delta(z)$, in the model equations.

One important ice property that is derived from the density is the porosity, $s(z)$, which is the proportion of void space in the firn or ice. Thus

$$s(z) = 1 - \rho(z)/\rho_i \tag{3.3}$$

The void described by the porosity is divided into open and closed (or "free" and "trapped") porosity, $f(z)$ and $b'(z)$, where

$$s(z) = f(z) + b'(z) \tag{3.4}$$

For each site the free and trapped porosities are assumed to depend only on the density. The trapped volume is expressed as $b'(z) = r(z)s(z)$, where $r(z)$ goes from virtually zero at the surface to 1 at and below the firn-to-ice transition. Of greater importance for gas trapping calculations is $b(z)$, which is $b'(z)$ converted back to ambient pressure. The relationship of $b'(z)$ to $b(z)$ is given by the compression parameterization.

Representation of the diffusion is based on the work of Schwander and all diffusion is related to the diffusion of CO_2. For each species, X, the diffusion coefficient of X in air relative to the diffusion coefficient of CO_2 in air, γ_X, is required. This is multiplied by the diffusivity of CO_2 through the air-filled channels in the firn to give the diffusion coefficient, $D(z)$, of the particular species. The diffusivity at different depths in the firn is defined to be a function of density (or density-related quantities such as porosity). The possibility of melt layers in the firn is also considered. A melt layer is modelled as a layer that moves with the firn or ice and through which diffusion is reduced. The effect of the melt layer due to chemistry is neglected.

Finally, the free and trapped trace gas concentrations are defined as the amount of trace gas per unit open volume for the free concentration and per unit closed volume for the trapped concentration. These concentrations are denoted $C(z,t)$ and $X(z,t)$, respectively. The task of the model is to calculate these concentrations given the surface concentration, $C_0(t)$. In most cases, however, trace gas measurements are determined as mixing ratios rather than concentrations. Therefore, for ease of comparison with observations, the model equations are formulated to give values of the trace gas mixing ratios in the free and trapped air, denoted by the lowercase letters $c(z,t)$ and $\chi(z,t)$. The cases discussed give model results as trace gas mixing ratios.

3.3.1 Basic equations

Schwander (1989) introduced the basic gas diffusion equations for the concentration $C(z,t)$ of a trace gas in terms of $J(z,t)$, the flux through open firn channels,

$$J(z) = -D(z)\left[\frac{\partial C}{\partial z} - \frac{MgC}{RT}\right] \tag{3.5}$$

Here, $D(z)$ is the gas diffusion coefficient, M is the molecular weight, g is the acceleration due to gravity, R is the gas constant, and T is temperature. The term MgC/RT gives the settling due to gravity.

The change of concentration can be derived from the flux divergence by virtue of conservation of mass, which has to be applied in terms of the full space where the derivatives are defined and not in terms of the open volume. In terms of the full volume the flux (amount of gas flow per unit area) is $f(z)\,J(z,t)$, and the amount of gas per unit volume is $f(z)\,C(z,t)$.

Mass conservation takes the form

$$\frac{\partial}{\partial t}[f(z)\,C(z,t)] = -\frac{\partial}{\partial z}[f(z)\,J(z,t)] - \lambda f(z)\,C(z,t) \tag{3.6}$$

where λ is the radioactive decay rate of unstable species such as $^{14}CO_2$. If we assume that the term involving $\partial f/\partial t$ is negligible, then this is equivalent to

$$\frac{\partial C}{\partial t} = -\frac{\partial}{\partial z}J(z,t) - \lambda C(z) - \frac{1}{f(z)}\frac{\partial f}{\partial z}J(z,t) \tag{3.7}$$

The neglected term describes the upward flux of air relative to the firn due to the compression of pore space as the firn moves down into regions of lower open porosity. This flux is assumed to be negligible in comparison with the fluxes due to molecular diffusion (Schwander et al., 1988; Schwander, 1989). Our formulation differs from Schwander's in the explicit inclusion of the last term in equation (3.7). This term reflects the fact that, where the amount of open channel decreases with depth, a uniform flux per unit area of open channel leads to an accumulation of gas. The dependence on $f(z)$ indicates that this term will become important near the close-off region. Schwander's model uses a modified z coordinate in equation (3.6) with equal amounts of free gas in each layer, which avoids the need for this extra term.

Equation (3.5) has neglected the effect of bulk motion of the firn. Including this leads to the modified expression

$$J(z) = -D(z)\left[\frac{\partial C}{\partial z} - \frac{MgC}{RT}\right] + v\,C \tag{3.8}$$

where $v(z)$ is the vertical velocity (in meters per year) at depth z. To allow for this vertical advection, a moving coordinate system, which moves down at velocity, v, relative to the surface, is used. This approach is formally equivalent to the use of (3.8) in a fixed coordinate system. However, in constructing a finite difference approximation the use of moving coordinates allows greater accuracy for a given degree of discretization.

The above equations give results as concentrations, $C(z,t)$. However, as actual measurements are generally in terms of mixing ratios, the model output needs to be converted to mixing ratios using the air pressure in the firn column. The variation of air pressure with depth in the open pores is given by the barometric equation,

$$C_{\rm air}(z)/C_{\rm air}(0) = \exp(gzM_{\rm air}/RT)$$

but keeping track of air pressure in the closed pores is not trivial. To avoid this problem the model calculates the trace gas amounts as mixing ratios, $c(z,t) = C(z,t)/C_{\rm air}(z)$. Appendix 3-1 describes how the model equations can be formulated to give results as mixing ratios.

The mass conservation equation is written in terms of mixing ratio as

$$\frac{\partial c}{\partial t} = -\frac{\partial}{\partial z}J_M(z,t) - \lambda c(z) - \frac{1}{f(z)}\frac{\partial f}{\partial z}J_M(z,t) - J_M\frac{M_{\rm air}g}{RT} \tag{3.9}$$

where J_M, the mixing ratio flux, is defined as

$$J_M(z) = -D(z)\left[\frac{\partial c}{\partial z} - \frac{(M - M_{\rm air})\,gc}{RT}\right] \tag{3.10}$$

This is solved subject to a specified time series of mixing ratio at the surface, $c(t)$. The main difference in the model equations for mixing ratio compared with those for concentration is that the mass difference from air, $M - M_{\rm air}$, rather than the actual mass, M, in the gravity term of the diffusion equation must be considered. The extra term in the mass conservation equation appears to have negligible effect on the model results.

A recent model of firn diffusion and trapping by Rommelaere et al. (1997) writes the conservation equations for air and a trace gas in a coordinate system that is stationary

relative to the surface. They have a downward flux of air in this coordinate system that balances trapping of air into bubbles at the bottom of the firn. They stress that this flux is not equal to the velocity of the firn layers, and not due to interactions between gas molecules and pore walls. Their downward flux of air is smallest near the surface where air compression is greatest and increases with depth through the firn. It takes into account the upward flux due to compression mentioned above that has been neglected by other models.

3.3.2 Finite difference implementation

The diffusion equation is solved numerically by using a finite difference representation. A vertical column of firn and ice is divided into horizontal layers, each having an equal mass of ice or firn per unit area. W denotes this quantity, which is expressed in kg m^{-2} per layer. Nominally, the model considers N layers. The use of moving coordinates means that $N-1$ full layers and a surface layer whose ice content varies from zero to W are used. From the definition of the accumulation rate, A, each new layer accumulates in a time $\tau = W/A$ (in years). The time interval τ is divided into an integer number of model time steps. Initially, the surface layer (layer 1) has a mass of zero, and after time τ the mass in this layer reaches W. At this point the coordinate system is relabeled, putting the values (c_m, χ_m, σ_m) into $(c_{m+1}, \chi_{m+1}, \sigma_{m+1})$, and layer 1 once again becomes a layer of zero mass. This procedure is repeated for each time interval, τ.

After a time t the coordinate system will have moved t/τ boxes relative to the surface. The fractional part of this distance is denoted by ϕ, and it describes the position of the coordinate system with respect to its initial position. The input quantities, density ρ, and depth z, are specified on this initial fixed coordinate system, and these values are linearly interpolated by using ϕ to calculate the corresponding values on the moving coordinate system.

The densities and depths in the moving coordinate system are calculated at both the center and the boundary of each layer. A tilde indicates when they correspond to layer centers. Other model quantities are determined from these (either by parameterizations or by modelling) at layer centers, layer boundaries, or both. The same index, m, is used to denote the center of a layer and its lower physical boundary. Thus boundary m separates layers m and $m+1$. The quantities defined at the cell boundaries are the flux, J_m, and

diffusion coefficient, D_m. Those defined at cell centers are free and trapped mixing ratios c_m and χ_m, depth z_m, and layer thickness Δ_m. Open and closed porosities, f_m and b_m, are defined for both centers and boundaries, with the tilde again indicating layer centers.

The time rates of change of the c_m are integrated by using an Euler predictor-corrector scheme applied to the finite difference form of (3.9). Equation (3.10) is discretised as

$$J_m = -D_m \left[\frac{c_{m+1} - c_m}{z_{m+1} - z_m} - \frac{(M - M_{\text{air}})g}{RT} \frac{1}{2}(c_m + c_{m+1}) \right] \quad \text{for } m = 2 \text{ to } N-1 \tag{3.11}$$

to give J_m, the flux at boundary m, where D_m is the diffusion coefficient.

The fluxes across the surface and boundary 1 are

$$J_0 = -D_0 \left[\frac{c_2 - c_0}{z_2} - \frac{(M - M_{\text{air}})g}{RT} c_0 \right] \tag{3.12}$$

$$J_1 = -D_1 \left[\frac{c_2 - c_1}{z_2 - z_1} - \frac{(M - M_{\text{air}})g}{RT} \frac{1}{2}((2 - \phi)c_1 + \phi c_2) \right] \tag{3.13}$$

In this form the model requires a very small time step to remain stable. In order to be able to increase the time step to a more manageable value, a flux smoothing technique is employed. Fluxes are smoothed according to

$$J_m = a_1 J_{m-1} + a_2 J_m + a_1 J_{m+1} \tag{3.14}$$

where $a_1 = 0.15$ and $a_2 = 0.7$ give the most stable results. There is negligible difference between the solution with and without smoothing. The flux at boundary 1 is smoothed by using

$$J_1 = a_1 \phi J_0 + a_2 J_1 + (1 - a_2 - a_1 \phi) J_2 \tag{3.15}$$

The mixing ratio in layer 1 is not specifically modelled. The thickness of this layer varies, and for small thicknesses the model would become unstable. Instead, c_1 is calculated by linear interpolation between layer 2 and the prescribed surface mixing ratio, c_0, taking into account the varying size of layer 1. The flux across the surface, J_0, is therefore not used directly to calculate c_1; however, since it is used in the flux smoothing for J_1, it still must be calculated.

A melt layer in the firn is modelled by reducing the flux across the boundary between two layers, r and $r+1$. The flux is set to $J_r^m = wJ_r$, with $0 \leq w \leq 1$, where the value of

r is given by the integer part of $(t - t_{\rm melt})/\tau$ (i.e., the melt layer moves with the model layers), and $t_{\rm melt}$ is the time when the melt layer is formed at the surface. The value of w is the degree to which the melt layer reduces the diffusive flux. The flux J_r^m is not involved in the flux smoothing described above.

The above equations apply for the free trace gas mixing ratios, c_m. For the trapped trace gas mixing ratios, χ_m, only the processes of radioactive decay and trapping need to be modelled. The trapped concentration evolves as new pores close off and is calculated by averaging the current trapped concentration with the concentration in the newly trapped volume (i.e., the free concentration).

3.4 Inputs to the model

3.4.1 Ice cores

The firn model is applied to a number of sites, covering a wide range of accumulation rates and temperatures. Table 3.1 gives some of the measured characteristics for the sites that are considered. The model is developed and tested using mainly firn measurements from DE08. The DE08 measurements come from 2 cores: DE08 drilled in 1987 (Etheridge and Wookey, 1989) and DE08-2 drilled in 1993 (Etheridge et al., 1996). DE08 and DE08-2 are on the east side of Law Dome, East Antarctica, separated by about 300 m, and have a very high accumulation rate (1100 kg m^{-2} yr^{-1}). The high accumulation rate means that the air trapped in the ice has a small age spread, so atmospheric records can be determined with fine resolution in time. During the drilling of DE08-2, samples of air were collected from the firn layer, and a number of trace gases and isotopic ratios have been measured. These data allow investigation of air mixing processes in the firn. Air extracted from the ice at DE08 and DE08-2 holds information about the composition of the atmosphere dating back to about 1830 (Etheridge et al., 1992; 1996). The most recent ice core air (about 1978) overlaps with direct atmospheric sampling for some species, allowing validation of the diffusion and bubble trapping processes. The DE08 and DE08-2 ice and firn were measured for density and porosity (Etheridge and Wookey, 1989; Barnola et al., in prep.).

DSS is a lower-accumulation-rate site on Law Dome (Etheridge, 1990; Morgan et al., 1997). DSS was drilled in sections from 1988-93 down to bedrock, and measurements from DSS extend the Law Dome CO_2 and $\delta^{13}C$ ice core record back to 1006 (Etheridge

et al., 1996; Francey et al., 1999a). Another core, DSS97, was drilled near DSS in 1997. Firn air was sampled at DSSW20K (20 km west of DSS) in the summer 1997/98 (D. Etheridge, pers. comm.). Siple Station, West Antarctica, has been measured for many physical parameters and air composition (Neftel et al., 1985; Schwander et al., 1988). Firn air dating back to the start of the 20$^{\text{th}}$ century was collected at South Pole (Battle et al., 1996). Summit, Greenland provides a northern hemisphere site with many supporting measurements (Schwander et al., 1993). Vostok is a very low accumulation site, and because of this the ice cores give records with coarse resolution in time but extending a long way (more than 400,000 years) into the past (Petit et al., 1999). The low accumulation rate leads to a wide age spread of the enclosed air, due to the longer trapping time.

Core	Location	A, kg m^{-2}yr^{-1}	P, hPa	T, K	ρ_0, kg m^{-3}
DE08, DE08-2	East Antarctica	1100[a]	850[b]	254[b]	340[c]
DSS, DSS97	East Antarctica	600[a]	825[d]	251[a]	400[e]
DSSW20K	East Antarctica	150[l]	850[l]	252[l]	350[l]
Siple Dome	West Antarctica	137[f]	850	248[f]	350[f]
Siple Station	West Antarctica	500[g]	867[h]	249[g]	350[h]
Sth Pole	Antarctica	74[f]	681[f]	224[f]	410[f]
Summit	Central Greenland	209[i]	665[i]	242[i]	340[i]
Vostok	Central East Antarctica	22[g]	624[j]	216[g]	350[k]

Table 3.1: Firn parameters for the cores investigated using the model. References: [a]Etheridge et al. (1996); [b]Etheridge et al. (1992); [c]Li et al. (1991); [d]Automatic weather station data (I. Allison, pers. comm., 1995); [e]Extrapolation of density measurements (unpublished data of Australian Antarctic Division); [f]M. Battle (pers. comm., 1998); [g]Schwander and Stauffer (1984); [h]Schwander (1984); [i]Schwander et al. (1993); [j]Martinerie et al. (1992), corrected to apply at surface using barometric equation; [k]J.-M. Barnola (pers. comm., 1995). [l]D. Etheridge (pers. comm., 1998).

3.4.2 Specification of ice properties

The model requires profiles of the density, porosity, and diffusivity in the firn to calculate the diffusion and bubble trapping. These input quantities can be obtained by using models (either empirical or mechanistic) or from curves fitted to measured data.

Density: A key parameterization in the model is that of density versus depth, and there are a number of ways in which this can be determined. The Herron-Langway model (Herron and Langway, 1980) and the Pimienta model, described by Barnola et al. (1991),

are two examples of empirically based density parameterizations. These parameterizations determine the density variation with depth for a site given its temperature, accumulation rate, and surface density, and they are useful when measured values are not available. Fortunately, density is often measured so for most of the sites used in the model smoothing spline fits to the measurements are used. The splines are biased toward the higher-density values at each depth, because it is these values that will limit the diffusion. Figure 3.2 shows density profiles for DE08 and DE08-2 with measurements from Etheridge and Wookey (1989) and Barnola et al. (in prep.).

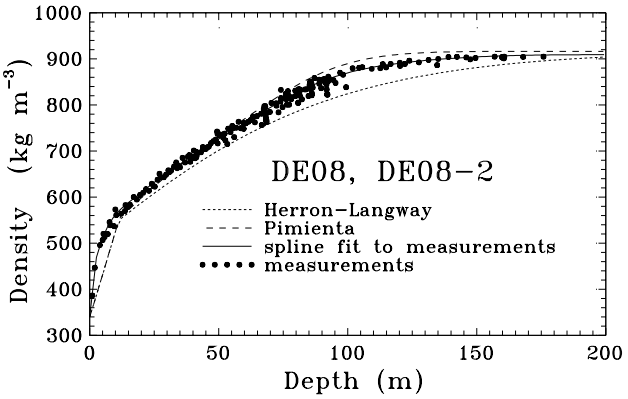

Figure 3.2: Density profiles for the DE08 and DE08-2 sites calculated with the Herron-Langway model and the Pimienta model, as well as measured values and a smoothing spline fit to measurements.

Porosity: Open and closed porosities in the firn are related to the density. Where measurements exist (DE08, Vostok and Summit) curves fitted to the porosity measurements as a function of density are used. For other sites, the spline fit for the site with the closest accumulation rate and temperature is used. Figure 3.3 shows DE08 closed porosity data from Barnola et al. and the spline fit used in the DE08 and DE08-2 model calculations. When measured porosity is not available, the empirical relation from Schwander (1989) or alternatively, percolation theory (Enting, 1985; 1987) can be used to relate the closed porosity to the density.

Diffusion: The diffusion coefficient, $D(z)$, for a species X is characterised by the diffusion coefficient of X in air relative to CO_2 in air, γ_X, multiplied by the diffusivity of

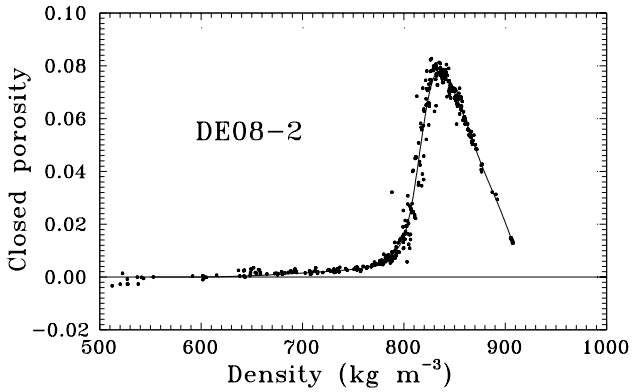

Figure 3.3: Spline fit to DE08 closed porosity versus density data of Barnola et al. (in prep.).

CO_2 in the firn.

The diffusion coefficients for some of the species considered come from Marrero and Mason (1972), who give semi-empirical approximations for the composition dependence and temperature dependence of the diffusion coefficient. The approximations are based on measurements from a number of different studies. For species not given by Marrero and Mason the following formula from Perry and Chilton (1973), is used

$$D_{12} = \frac{B(M_1, M_2)T^{\frac{3}{2}}\sqrt{(1/M_1) + (1/M_2)}}{Pr_{12}^2 I_D} \tag{3.16}$$

where D_{12} is the diffusion coefficient of component 1 in component 2,

$$B(M_1, M_2) = 10.85 - 2.50\sqrt{(1/M_1) + (1/M_2)} \times 10^{-4}$$

T is absolute temperature, M_1, M_2 are molecular weights of components 1 and 2, P is pressure, r_{12} is the collision diameter, and I_D is the collision integral for diffusion and is a function of temperature and species. This expression was given by Hirschfelder et al. (1954) with $B = 9.2916 \times 10^{-4}$ as the first approximation to the diffusion coefficient in a binary mixture. The linear expression for B given above was determined by Wilke and Lee (1955) from a comparison of experimental results with Hirschfelder's equation. (A table of the collision integral is given by Perry and Chilton (1973), as well as the collision diameter, r_{12}, and the force constant, ϵ/k, needed to calculate the collision integral.) Table 3.2 gives

X	γ_X
CO_2	$\equiv 1.000$
CH_4	1.291
CO	1.2696
N_2	1.268
O_2	1.268
SF_6	0.583
N_2O	1.004

X	γ_X
CFC-11	0.5498
CFC-12	0.6121
$^{13}CO_2$	0.9958
$^{14}CO_2$	0.9918
$^{13}CH_4$	1.2683
$^{14}N^{15}N$	1.257
$^{16}O^{18}O$	1.2516

Table 3.2: Scale factors for diffusion coefficients. The first five values on the left were calculated by using data from Marrero and Mason (1972), and the rest were calculated using equation (3.16).

values of γ_X at $T = 253$ K and $P = 1$ atm. $D_0 = 0.1247$ cm^2 sec^{-1} is used for the diffusion coefficient of CO_2 at this temperature and pressure. (The values for N_2 and O_2 are for N_2 diffusing in O_2 and O_2 diffusing in N_2, and since $D_{12} = D_{21}$, they are therefore both the same.)

The temperature and pressure dependence from equation (3.16) is used to convert these ratios at 253 K and 1 atm to apply at the required temperature and pressure, i.e.,

$$\frac{D(T_2, P_2)}{D(T_1, P_1)} = \left(\frac{T_2}{T_1}\right)^{1.5} \frac{I_D(T_1)}{I_D(T_2)} \frac{P_1}{P_2} \tag{3.17}$$

The mass dependence of equation (3.16) is used to determine the mass correction for minority isotopes (e.g., for $^{13}CO_2$, $^{13}CH_4$, $^{14}N^{15}N$). The ratio of the diffusion coefficients of two isotopes of the same species with masses M_1 and M_2 is given by

$$\frac{D(M_2)}{D(M_1)} = \frac{\sqrt{\frac{1}{M_2} + \frac{1}{M_{\text{air}}}}\,(10.85 - 2.50\sqrt{\frac{1}{M_2} + \frac{1}{M_{\text{air}}}})}{\sqrt{\frac{1}{M_1} + \frac{1}{M_{\text{air}}}}\,(10.85 - 2.50\sqrt{\frac{1}{M_1} + \frac{1}{M_{\text{air}}}})} \tag{3.18}$$

where $M_{\text{air}} = 28.966$ g is the mass of air. This ratio differs from the commonly used ratio of the square root of the reduced masses by the empirically determined factor $B(M_1, M_2)$, discussed above.

The work of Schwander uses the following temperature and pressure dependence for the diffusion coefficient:

$$\frac{D(T_2, P_2)}{D(T_1, P_1)} = \left(\frac{T_2}{T_1}\right)^{1.85} \frac{P_1}{P_2} \tag{3.19}$$

and $D_0 = 0.14$ cm^2 sec^{-1} for the value of the diffusion coefficient at $T = 253$ K, $P = 1$ atm. The temperature dependence from equation (3.17), when written in the form of

equation (3.19), corresponds to values of the exponent approximately in the range 1.80–1.95 for relevant temperatures and species.

The dependence of CO_2 diffusivity on open porosity is the most uncertain of the model input functions. Schwander uses a linear dependence of the diffusivity on open porosity (Schwander et al., 1988; Schwander, 1989),

$$D(z) = D_0[1.7f(z) - 0.2] \qquad \text{for } f(z) > 0.12 \tag{3.20}$$

where D_0 is the diffusion coefficient of the considered gas in air. This equation is based on measurements of the Siple core. The firn model will be used to tune the relationship between CO_2 diffusivity and open porosity, taking advantage of the fact that the DE08-2 firn contains air that overlaps with the record of direct observations for a number of species. The data used to determine the DE08-2 diffusivity relation is described in Section 3.5.1. Figure 3.4 shows this relationship, along with the Siple linear dependence.

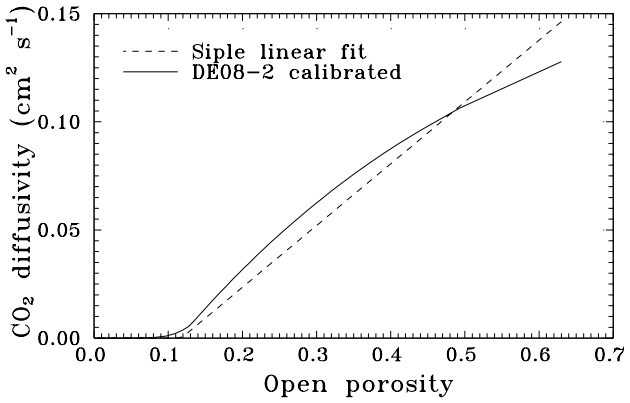

Figure 3.4: Dependence of CO_2 diffusivity in the firn on open porosity. The dashed line shows the linear relationship given by Schwander et al. (1988) for Siple. The solid line is the diffusivity tuned to give the best fit to the DE08-2 firn CO_2 and SF_6.

There are important advantages to tuning the diffusivity with the model, rather than using a diffusivity profile based on measurements. As Etheridge (1999) points out, measurements of diffusivity on core samples may not be representative of the actual diffusion that occurs *in situ* in the firn. Fabre et al. (2000) also suggest that tuning the model is preferable to using diffusivity measurements on small samples, because diffusivity depends on porosity which is not always known.

3.5 Model calculations for DE08-2

In this section, a number of model calculations are described. The model is tested and diffusivity calibrated using measurements from the DE08-2 firn. This is followed by discussion of the effects of gravity, age distributions and effective age. At the beginning of a model run, the tracer mixing ratios in the firn and ice are initialised to the starting atmospheric value. The model must then be run for long enough to establish the gradient in the firn. This process takes around 10 years for DE08-2. The model calculations described here are integrated for at least 50 years. The resolution of the model runs for DE08-2 is usually quite coarse, with model layers corresponding to annual ice layers (i.e. W = 1100). The timestep used is 0.005 yr. The model can be run with or without gravitational separation, by including or excluding the relevant term from the model equations. The calculations for the age distributions and the diffusion correction are run without gravitational separation. When isotopic ratios are modelled in the firn, the model calculates the mixing ratios of the two isotopes as separate tracers diffusing through the air-filled channels, and at the output stage combines them to give the isotopic ratio. For example, $\delta^{15}N_2$ is calculated by modelling $^{14}N^{15}N$ and $^{14}N^{14}N$.

3.5.1 Firn air composition

The DE08-2 firn and upper ice layers contain air that overlaps with the record of direct atmospheric observations, and this overlap allows calibration of the diffusion processes in the model. Etheridge (1999) describes the sampling and measurement of the air composition in the firn layer at DE08-2 in the summer 1992/1993. Measurements of CO_2, CH_4, and SF_6 are used in this section.

The firn model is run by using known atmospheric records, and the modelled firn mixing ratios are compared with the observations. The atmospheric records used are as follows.

1. CO_2: measurements from South Pole in the Scripps Institution of Oceanography air sampling network (Keeling and Whorf, 1994). For CO_2 values prior to 1957 we use a spline fit to DE08, DE08-2, and DSS ice core data (Etheridge et al., 1996).

2. CH_4: zonal average for 60°–90°S from the global methane "flying carpet" derived from the NOAA Climate Monitoring and Diagnostics Laboratory global cooperative air

sampling network (Dlugokencky et al., 1994; E. Dlugokencky, pers. comm., 1994). CH_4 prior to 1983 is taken from Etheridge et al. (1992).

3. SF_6: $c(t) = 0.003921(t - 1966.89)^2$ for $t \geq 1966.89$. This function is from Maiss et al. (1996), where t is time in years AD. The equation is based on direct measurements of SF_6 at the southern hemisphere stations Cape Grim, Tasmania (40°S), and Neumayer Station, Antarctica (70°S), and includes measurements of archived air samples from Cape Grim (Langenfelds et al., 1996).

The firn and ice properties used in the following runs are given by spline fits to measured density and porosity data. For the diffusivity versus open porosity dependence, Schwander's linear fit to the Siple data (equation 3.20) was used as a starting point, and the DE08-2 firn SF_6 and CO_2 data were used to tune the diffusivity to improve the fit to these trace gases. The diffusivity was tuned by manually altering the diffusivity at different depths until the modelled mixing ratios matched observations.

The SF_6 and CO_2 in the first 10 m of the firn required special attention. The difference between the measured SF_6 at the surface and 10 m is 0.51 parts per trillion. By using the SF_6 quadratic function to determine age this value corresponds to an age difference of 2.3 years. The gradient in SF_6 below 10 m is much less than that above 10 m. To reproduce this difference, the model would need low diffusivity above 10 m and higher diffusivity below. The CO_2 also has a gradient steeper than that expected in the first 10 m, although because of the seasonal cycle and smaller growth rate the discrepancy for CO_2 is not as obvious as that for SF_6. Stratigraphy of the DE08-2 core reveals that there was a melt layer in the DE08-2 firn at around 8.9 m in 1993, corresponding to the 1989/1990 summer (Etheridge, 1999). Temperature records for Law Dome show anomalously warm temperatures at this time (I. Allison, pers. comm., 1995). Although occasional thin melt layers are observed in the DE08 and DE08-2 cores, this is by far the most significant melt layer, and it appears from the firn air composition that it has had a major effect on the diffusion. The melt layer was incorporated into the model as described in Section 3.3.2. The amount by which the melt layer reduces the diffusive flux in the model was tuned by matching primarily the modelled SF_6, but also CO_2, with observations and was found to be approximately 80 %.

The atmospheric records of CO_2 and SF_6 have quite different characteristics. CO_2

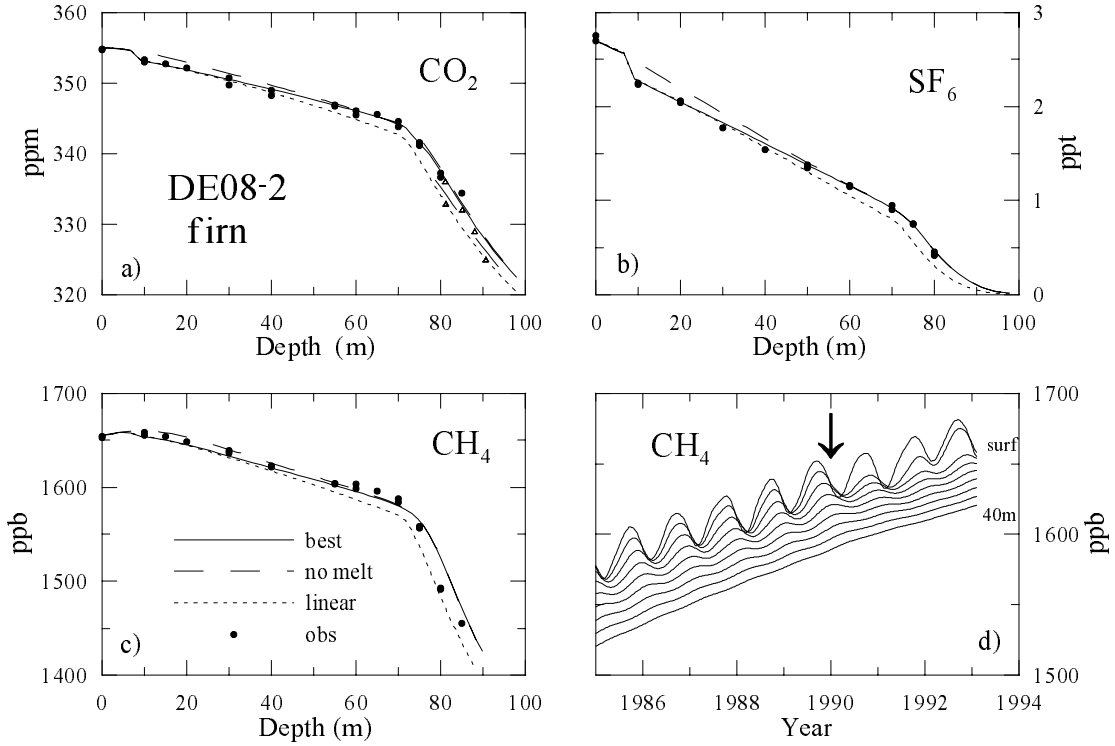

Figure 3.5: Modelled and observed concentrations of a) CO_2, b) SF_6 and c) CH_4 in the DE08-2 firn. The solid line shows the best model fit, using the DE08-2 calibrated diffusivity and with a melt layer that moves from the surface in 1990 to 8.7 m in 1993. The short dashes show the model calculations for linear diffusivity versus open porosity, and the medium dashes show the calculation without a melt layer. In a) the long dashes show modelled CO_2 trapped in the ice, and the triangles show ice core measurements. d) Time series of modelled CH_4 between the surface and 40 m at depth intervals of 5 m in the DE08-2 firn. The arrow indicates approximately when the melt layer was at the surface.

variation is close to linear over the period of interest, with a small seasonal cycle. SF_6 has increased 2 orders of magnitude since 1970 and has no seasonal cycle. The large growth rate gives SF_6 a high signal-to-noise ratio, which makes it a good trace gas for calibrating models. The errors on the SF_6 data are quite small (about 1 %), giving confidence in the estimate of the effect of the melt layer on the diffusion and the dependence of diffusivity on open porosity.

The model also gives a good fit to DE08-2 CH_4 data. Figures 3.5a, b and c show modelled and observed values of SF_6, CO_2 and CH_4 for the DE08-2 firn. Figure 3.5a also shows the observed and modelled CO_2 concentrations for the upper layers of the ice. The model predicts a difference between the trapped and free mixing ratios in the firn to ice

transition region. This is also observed in the measurements, and it occurs because the trapping takes place over a range of depths, giving the trapped air a slightly different mean age in comparison with the air that is still mixing. In the model this result depends very much on the diffusivity parameterization. Reasonable agreement between modelled and observed CO_2 in the ice gives some confidence in the model inputs that control the relative timing of the diffusion and bubble trapping. A more rigorous test on these inputs can be provided by species with faster atmospheric changes, such as the $^{14}CO_2$ pulse due to nuclear weapons tests in the 1950s and 1960s. A comparison of $^{14}CO_2$ measurements and model results will be discussed in Section 3.7.1.

The modelled SF_6, CO_2, and CH_4 calculated by using the "DE08-2" diffusivity and the 1990 melt layer are in excellent agreement with the DE08-2 observations. The CH_4 firn measurements near the surface show a slight increase with depth because sampling was done at about the minimum in the seasonal cycle. Figure 3.5d shows time series of modelled CH_4 from the surface to 40 m at depth intervals of 5 m in the DE08-2 firn. The seasonal cycle of CH_4 in the atmosphere in the southern hemisphere is quite large in comparison with the mean growth rate, and the model predicts that it penetrates to about 30 m in the firn. The arrow in Figure 3.5d indicates approximately when the melt layer was at the surface. The bigger differences between the surface, 5 m and 10 m curves at each maximum after 1990 compared with before 1990, show the effect of the melt layer on the mixing as the layer moves downward with the ice.

3.5.2 Gravitational fractionation

Gravity plays quite a significant role in distributing the air within the firn column, and it is important that it is correctly represented in the firn diffusion model. If the firn column was in perfect diffusive equilibrium, then the concentration of any gas with constant surface concentration would follow the barometric equation

$$\frac{C}{C_0} = \exp \frac{Mgz}{RT} \tag{3.21}$$

where C_0 is the surface concentration and M, g, z, R, and T are as for equation 3.5 (Craig et al., 1988; Schwander, 1989; Sowers et al., 1989). The concentration of any species therefore increases with depth at a rate that depends on its mass. This mass dependence causes heavier species to be enriched at depth compared with lighter ones. The

fractionation due to gravity is particularly apparent in considering ratios of components. The variation with depth of the ratio of two species in equilibrium is given by

$$\frac{C_1}{C_2} = \exp \frac{(M_1 - M_2)gz}{RT} \tag{3.22}$$

that is, it depends on the mass difference, $M_1 - M_2$, rather than the actual masses. The variation of mixing ratio with depth also follows this relationship, where M_2 is the mass of air, M_{air}. The mixing ratio of a species in equilibrium therefore increases with depth if $M_1 > M_{\text{air}}$ and decreases with depth if $M_1 < M_{\text{air}}$.

The equations used by the firn diffusion model include a term for the flux due to gravity. The best way to test that gravity is correctly represented in the model is to consider the ratio of two components in the firn that have constant surface concentrations. The isotopic ratios, $\delta^{15}N_2$ and $\delta^{18}O_2$, are measured in the firn in order to quantify the effect of gravity. N_2 (i.e., $^{14}N^{14}N$), O_2 ($^{16}O^{16}O$), and their isotopes $^{14}N^{15}N$ and $^{16}O^{18}O$ have been effectively constant over timescales much greater than those for firn diffusion.

Assuming that the column is in diffusive equilibrium, the ratio of $^{14}N^{15}N$ to N_2 can be written using the δ notation as

$$\delta^{15}N_2 = \left[\frac{\left(^{14}N^{15}N/N_2\right)_{\text{sample}}}{\left(^{14}N^{15}N/N_2\right)_{\text{reference}}} - 1 \right] \times 1000 \tag{3.23}$$

$$= \left[\exp\left(\frac{gz}{RT}\right) - 1 \right] \times 1000 \tag{3.24}$$

This equation can be considered to be a theoretical maximum for the ratio, as it assumes that the column is in perfect diffusive equilibrium. In reality, sites with low accumulation rates have $\delta^{15}N_2$ profiles that are closer to the theoretical curve than sites with high accumulation rates. Model runs give results that match this observation, confirming that it is mainly the vertical advection of the ice that prevents the column from reaching perfect diffusive equilibrium, as suggested by Sowers et al. (1989). The modelled $\delta^{15}N_2$ for DE08-2 is close to observations (Figure 3.6), verifying the gravitational fractionation in the model. The modelled values are calculated with the 1990 melt layer. $\delta^{15}N_2$ model calculations for Summit and Vostok firn are shown in Trudinger et al. (1997).

The $\delta^{15}N_2$ value gives a measure of the gravitational fractionation for a mass difference of 1 g/mol and is often used as a correction to remove the effect of gravity for other species (Sowers et al., 1989). In order to see whether the fractionation in the model

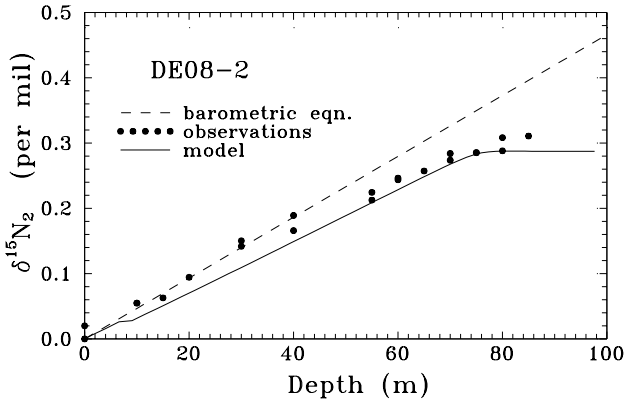

Figure 3.6: Observations and model calculation of $\delta^{15}N_2$ in the DE08-2 firn. The model calculation includes the 1990 melt layer (see Section 3.5.1 for details).

depends only on the mass difference, as expected, the model is used to calculate the gravitational fractionation for $\delta^{13}CO_2$ in the same way as was done for $\delta^{15}N_2$, i.e., with constant atmospheric levels of CO_2 and $^{13}CO_2$. The model gives slightly different isotopic ratio for the different species, even though the mass difference is the same. The ratio of $\delta^{13}CO_2$ to $\delta^{15}N_2$ at any depth is about 0.94 for DE08-2, while the ratio of $\delta^{13}CH_4$ to $\delta^{15}N_2$ calculated in the same way is about 1.04. For sites with accumulation rates lower than the one of DE08-2 this effect is reduced, and there is essentially no difference between the $\delta^{13}CO_2$, $\delta^{13}CH_4$, and $\delta^{15}N_2$ when the model is run without vertical advection of the ice. As already mentioned, it appears that the vertical advection of the ice prevents the firn column from reaching perfect diffusive equilibrium. The different diffusion rates of the tracers will determine how far out of equilibrium, i.e., how far from the barometric equation, each tracer is. The tracer masses appear also to play a part in explaining the differences.

In most cases this effect would be negligible. Only for sites with very high accumulation rates, and when the effect of gravitational fractionation is large, such as for isotopic ratios, would it need to be considered. Even though these differences are probably smaller than the errors on individual measurements, they may cause a systematic shift of the deeper firn values relative to the surface values and are therefore worth noting. The model was also used to calculate the gravitational fractionation for $\delta^{13}CO_2$ with realistic atmospheric

growth rates for CO_2 and $^{13}CO_2$, but it was found to differ little from the case with constant atmospheric levels.

3.5.3 Age distributions and effective age

The major reason for measuring the composition of air in the firn and ice is to recover information about the atmosphere in the past, and this requires some knowledge of the age of the air contained in the ice. The processes of diffusion in the firn and bubble trapping tend to smooth out the atmospheric record. The air at a particular depth therefore has an age distribution that depends on both the diffusion and bubble trapping. Schwander et al. (1993) ran their diffusion model with a rectangular pulse of 1 year in the atmosphere to determine the age distributions at various depths for Summit. Figure 3.7 shows similar calculations using the present model for CO_2 at DE08. (The melt layer is not included in these calculations, because the age distributions would then be different for different depths of the melt layer, therefore introducing additional time variation to the results. The calculations therefore relate to the DE08 site. These runs are performed without the gravity term in the model equations, assuming that the effects of gravity are understood and can be corrected for.) The second solid line in Figure 3.7 gives the age distribution of the trapped air at 80 m. The width of the age distribution of the trapped air in this case is mainly due to the diffusion in the firn rather than to the bubble trapping. The age distribution in the ice is determined by the diffusion process and by the time it takes for the bubbles to close off while the air is still mixing. Much of the trapping occurs after the diffusion has stopped, so air is locked in the ice until it is eventually trapped into bubbles. This result depends heavily on the relative timing of the diffusivity and porosity parameterizations. It is clear from this that, in addition to the accumulation rate, the diffusivity in the close-off region is critical in determining the smoothing due to bubble trapping. Further investigation of the age distributions at DE08 is given by Levchenko et al. (1996) using ^{14}C. They performed a least squares fit of a moving average of the ^{14}C bomb pulse in the atmosphere to measurements of ^{14}C in DE08 and DE08-2 ice, and estimated an age spread of 12.5 ± 1.5 years for CO_2 trapped in DE08 ice.

It is often desirable to give a single value rather than a distribution for the age of a species. This is referred to as the effective age, τ, and it is used to relate sample measurements to past atmospheric levels. The effective age of a species at depth z in the

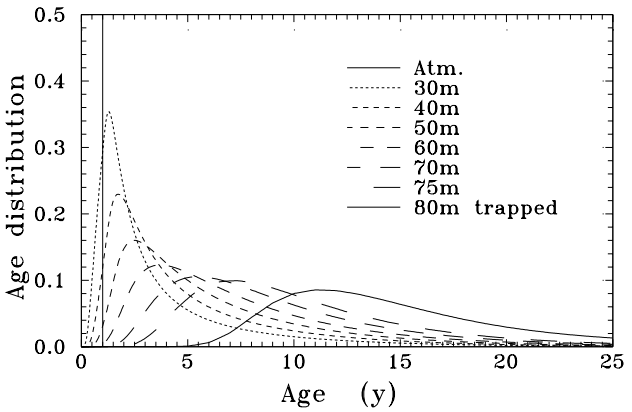

Figure 3.7: Age distributions of CO_2 molecules in the DE08 firn from the surface to 75 m, and in the ice at 80 m, calculated by using the diffusion model.

firn or ice can be defined as the elapsed time since the surface was at the same concentration as is currently seen at z, i.e., $C(z,t) = C(0, t-\tau)$. The concept of effective age becomes unclear when the atmospheric gradient disappears or changes sign, as there is no longer a unique value satisfying $C(z,t) = C(0, t-\tau)$ (Enting and Mansbridge, 1985). The diffusion model is used to investigate some features of the effective age.

The case for species that undergo linear growth in the atmosphere is quite straightforward. Figure 3.8a shows the effective ages of CO_2, CH_4, and SF_6 calculated with the model for linearly increasing atmospheric concentrations. Figure 3.8b shows model calculations of the effective ages of a number of species relative to the effective age of CO_2, assuming purely linear growth rates. Two cases are considered: no vertical advection of the ice and DE08 vertical advection. The calculations without advection show that the relative effective ages depend on the inverse of the relative diffusion coefficients of the species, as indicated by the solid line. When advection is included, the ratios shift toward 1.0. This shift depends on the rate of advection compared to the rate of diffusion of each tracer and is greater for faster advection (i.e., higher accumulation) and slower diffusion rates.

For species with atmospheric records that are not linear, the effective age depends also on the rate of atmospheric increase. This dependence implies that the effective age will vary as the atmospheric growth rate changes. The relationship between the effective ages

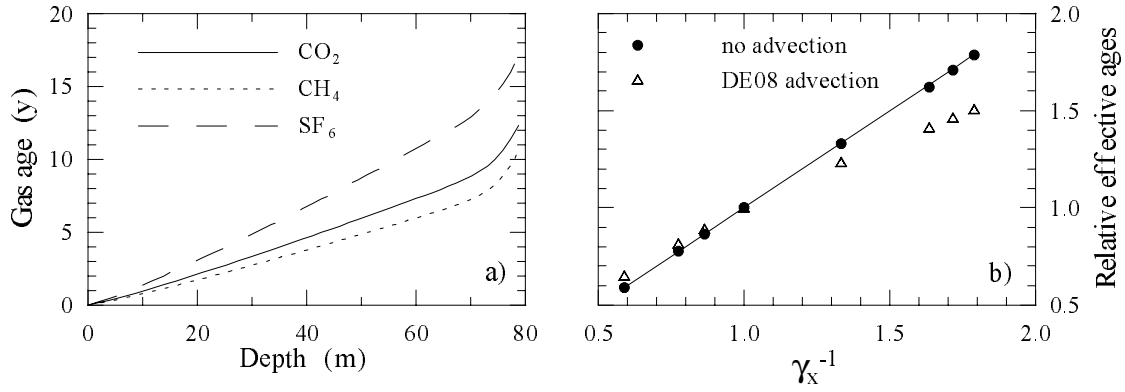

Figure 3.8: a) Effective ages of CO_2, CH_4 and SF_6 in the DE08 firn, assuming linearly increasing atmospheric concentrations. b) Effective ages of different species relative to the effective age of CO_2 plotted against the inverse of the relative diffusion coefficients. The solid line shows a linear relationship between relative age and the inverse relative diffusion coefficient.

of different species in the firn then becomes quite complicated. Further complication can be due to features in the ice that disrupt diffusive mixing, such as the 1990 melt layer in the DE08-2 firn.

An understanding of the variation of effective age with atmospheric growth rate can be useful for dating ice core measurements. Often an effective age is calculated for the base of the firn, and the air age–ice age difference is assumed to be constant below this. The age of the ice can usually be quite accurately determined by counting annual layers in $\delta^{18}O$, electroconductivity and hydrogen peroxide (Etheridge, 1999). The constant age difference assumption is normally a good first approximation, however it is not always the best estimate.

As an example, the firn model was run with an atmospheric record that consisted of a sinusoidal pulse of 10 years duration with linear increase before and after (solid line in Figure 3.9a). This function, when smoothed by diffusion and trapping, is meant to resemble a feature in the DE08 and DE08-2 CO_2 records around 1940-1950 (Etheridge et al., 1996) which will be discussed further in Section 3.7.1. The dashed line in Figure 3.9a is a concentration record reconstructed from the modelled (trapped) concentrations in the same way as the Law Dome ice core records are reconstructed. Ages are assigned to the modelled concentration profile using a constant air age – ice age difference of 30 years. This value was used by Etheridge et al. (1996) to date the DE08 and DE08-2 CO_2 ice

core measurements, and the linear parts of the concentration record in Figure 3.9a show that this value agrees well with the model (for constant growth rates in the atmosphere). The figure also shows that both the leading edge and the maximum of the pulse appear in the reconstructed record about 5 years earlier than in the original record. Although the concentration at the bottom of the firn at DE08 at time t is the same as the surface concentration at time $t - 10$ for a constant growth rate, a change such as a pulse at the surface effects the concentrations at the bottom of the firn much earlier than 10 years after they are seen in the atmosphere. This is a case in which the atmospheric growth rate has changed sign twice, but gradually enough that the feature is clear in the ice core record, although smoothed.

Another example where it is important to take into account variations in atmospheric growth rates is in dating tracers like SF_6 or CFCs which have a roughly exponential increase in the atmosphere. A number of such species have been measured in the DSSW20K firn (D. Etheridge, pers. comm.), and require effective ages for reconstruction of atmospheric records. Dating with a linearly increasing tracer in the model, or comparison with tracers such as CO_2 or CH_4 (which are approximately linear over the last few decades), gives a good first estimate of the effective ages, but it can be worthwhile refining these estimates by consideration of variations in the growth rate. For example, the model was

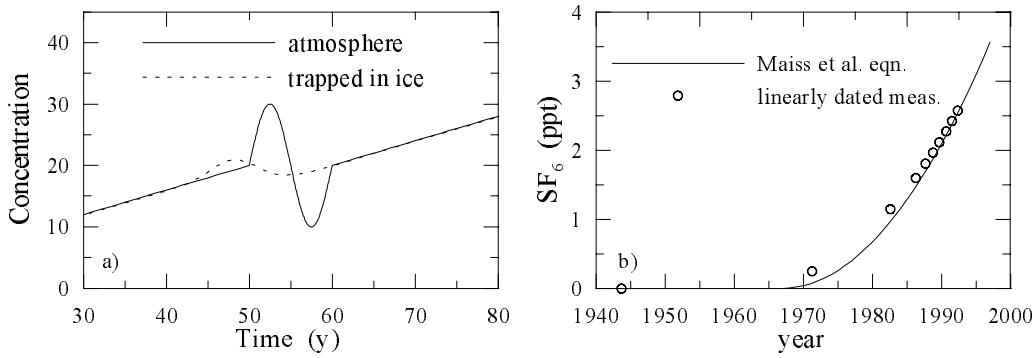

Figure 3.9: a) Hypothetical CO_2 record (solid line) and this record as it would be reconstructed from concentrations trapped in DE08 ice using a constant air age – ice age difference (dashed line). b) Solid line shows the SF_6 quadratic equation from Maiss et al. (1996). The circles show SF_6 concentrations from the firn model run for DSSW20K with the quadratic equation as atmospheric input, sampled at 5 m intervals in the firn and dated with a linear tracer in the model.

run for SF_6 in the DSSW20K firn with the quadratic equation for SF_6 from Maiss et al. (1996) (details of the DSSW20K inputs will be given in Section 3.8). The model output was 'sampled' at 5 m intervals, and these 'measurements' assigned dates calculated by the model with a linearly increasing tracer. The results are shown in Figure 3.9b, with the reconstructed record differing slightly from the original one. A second step of redating the 'measurements' using a record made up of a smooth fit to the circles in Figure 3.9b (i.e. running this curve as input to the model, and comparing calculated concentrations with the input to assign new dates) brings the reconstructed record very close to the original Maiss et al. input curve. Whether growth rate changes have an effect on effective age depends on the time scales of growth rate variations relative to the time scales of firn smoothing and trapping at a particular site.

The firn model has the capability to model seasonal variations in density, but this feature has not been used in the calculations described so far. Etheridge (1999) described the observed seasonal variation in density at DE08, and the likely implications of this for trapped air. The summer accumulation has a narrow layer with lower density and lower closed porosity than adjacent layers. Bubble close-off in these summer layers occurs later than in other layers, so the mean age of air contained in summer ice may be younger than that in other layers. Near the bottom of the firn, air may be sandwiched in the summer layers between the denser adjacent ice, and although not yet trapped may be sealed off from mixing vertically. The model was run for DE08 with the seasonally varying density shown in Figure 3.10a. A model layer thickness corresponding to 4 model layers per year of accumulation (i.e. 275 kg m^{-2} yr^{-1}) was used, and the results compared with a model run with the same resolution but without seasonality. In the seasonal case, the summer layers have lower density but the density of the other layers is the same as in previous runs (Figure 3.10b). As described in Section 3.3, the phase of the seasonality moves downward with the ice. The difference in density between summer layers and the rest is similar to the observed variation in the DE08 and DE08-2 density measurements (Figure 3.10a). The standard DE08 porosity and tuned diffusivity curves were used. Since porosity and diffusivity are functions of density, they also have seasonal variation versus depth. Figure 3.10a also shows the diffusivity versus depth with and without seasonality.

The model was used to calculate $\Delta^{14}CO_2$ in the ice around the time of the bomb

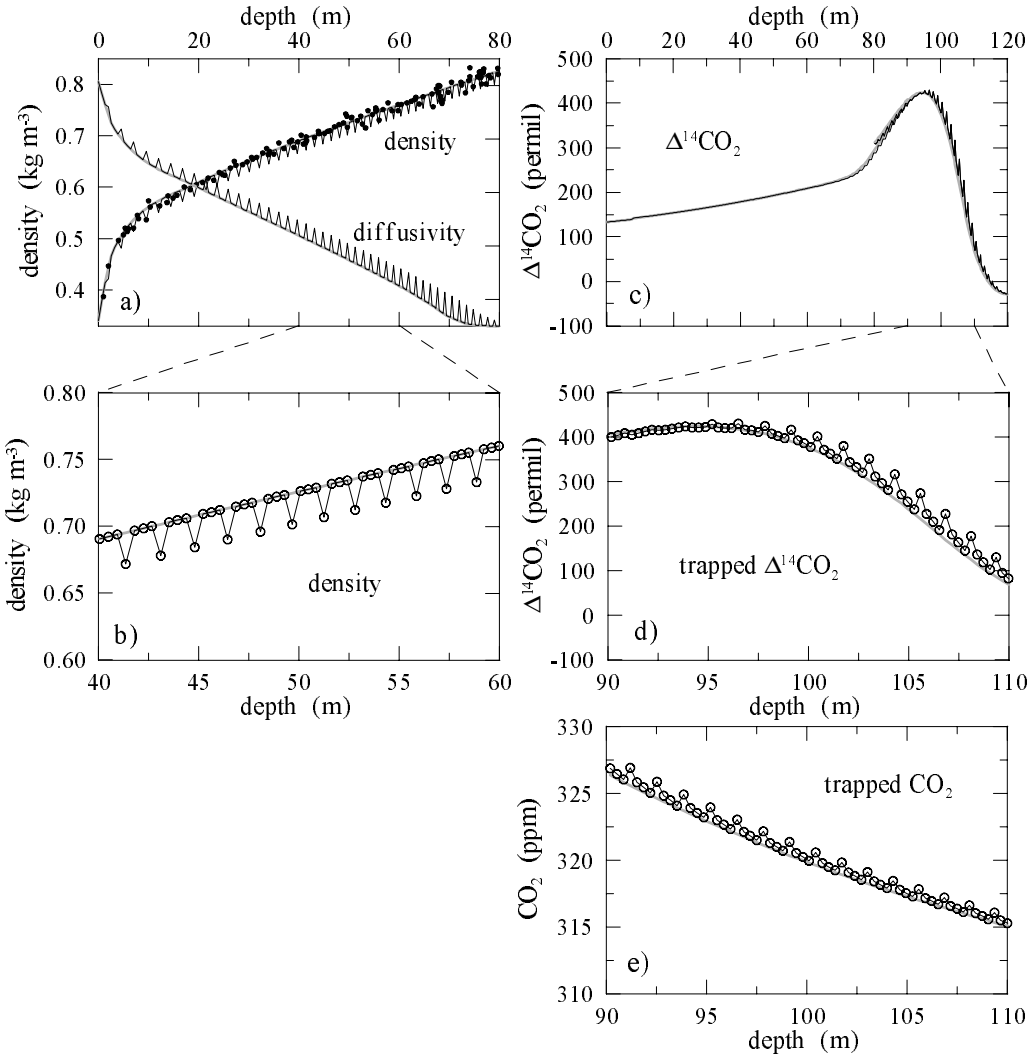

Figure 3.10: a) Density and diffusivity versus depth for DE08 with seasonal variation in density (thin line) and without seasonal variation (thick grey line). Symbols show DE08 and DE08-2 density measurements (Barnola et al., in prep.). (The scale for diffusivity is not shown.) b) Density versus depth as in part a) but between 40 and 60 m, with symbols showing each model layer for the seasonal density case. c) Modelled Δ^{14}C in the firn and ice, with (thin line) and without (thick grey line) seasonality. d) Modelled Δ^{14}C in the ice between 90 and 110 m, with symbols showing the Δ^{14}C in each layer for the seasonal case. e) Modelled CO_2 trapped in the ice, between 90 and 110 m with and without seasonality.

pulse. Figures 3.10c and 3.10d show the trapped and free Δ^{14}C calculated with and without seasonality. Δ^{14}C in the summer layers is more recent than that in the other layers, as expected. An important result is that the difference between non-summer layers and the run without seasonality is very small. The maximum difference in Δ^{14}C in

summer ice compared with that in the non-seasonal case is about 50 ‰. Through the firn where air is still mixing, the seasonal case is essentially the same as the non-seasonal case. Figure 3.10e shows modelled CO_2 with and without seasonality. The difference in concentration between summer and other layers depends on the rate of change of a tracer in the atmosphere. A model run with linear atmospheric CO_2 gives a CO_2 age difference of about 1 year between summer and non-summer ice. Etheridge et al. (1992) compared the CH_4 concentration in summer and non-summer ice to a smoothing spline to all measurements, and found an average age difference of 1.8 ± 0.8 years for summer ice. The Law Dome ice core CO_2 measurements (Etheridge et al., 1996) were selected from non-summer ice to avoid these difficulties with dating. The model calculations confirm that if the model is run with a density profile that matches non-summer density measurements, then calculations can be run without seasonality for comparison with concentrations in non-summer ice. The effect of seasonality at sites with lower accumulation rates may be greater than that at DE08, because the ice moves more slowly through the close-off region.

3.6 Diffusion correction for isotopic ratios

An important application of the firn modelling is to assess the effect of firn diffusion on the measured $\delta^{13}C$ in air in the firn and ice. The DE08-2 firn air $\delta^{13}C$ measurements cover roughly the same period as measurements from the Cape Grim Air Archive (Langenfelds et al., 1996), and this provides an excellent opportunity to confirm the results from the firn modelling. $\delta^{13}C$ in the firn is affected by gravitational settling in the same way as $\delta^{15}N_2$ as described in Section 3.5.2. In addition there is another effect that is important because the levels of CO_2 and $^{12}CO_2$ are changing in the atmosphere and can be explained as follows.

The isotopic ratio of a sample of firn or ice core air is actually the ratio of two isotopes with slightly different effective ages due to the mass dependence of the diffusion coefficient. For species with changing atmospheric levels, this measured ratio differs significantly from the ratio of the two isotopes with the same effective age, i.e., the true atmospheric value. In the case of $\delta^{13}C$, ^{12}C diffuses faster than ^{13}C in the firn, and therefore at any depth ^{12}C will have a younger effective age than ^{13}C, as illustrated in Figure 3.11. Even though the age difference between the two isotopes is very small (e.g. about 0.03 yr at 70 m), the

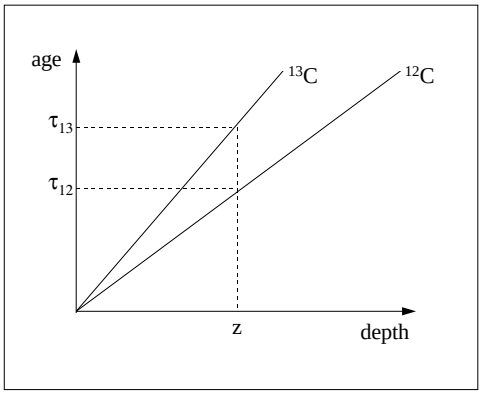

Figure 3.11: Schematic to demonstrate the different air ages of ^{12}C and ^{13}C due to the different diffusion rates in the firn.

isotopic ratio is very sensitive to changes in only one of the isotopes. This diffusion effect causes significant changes in isotopic ratios retrieved from firn and ice core air, and can be large compared to the actual rate of change in the atmosphere. A correction for this effect, referred to here as the *diffusion correction*, is required for reconstruction of atmospheric changes from firn or ice core measurements.

The diffusion correction will be calculated numerically with the model, however the following expression in terms of effective ages gives valuable insight into what most influences the correction. The isotopic ratio that we want to estimate from a measurement at depth z is

$$\delta^{13}(\tau_1) = \left[\frac{\frac{^{13}\mathrm{C}(\tau_1)}{^{12}\mathrm{C}(\tau_1)}}{r_s} - 1\right] \times 1000 \tag{3.25}$$

$$= \left[\frac{\frac{^{13}\mathrm{C}(\tau_2)}{^{12}\mathrm{C}(\tau_1)} + \frac{^{13}\mathrm{C}(\tau_1) - ^{13}\mathrm{C}(\tau_2)}{^{12}\mathrm{C}(\tau_1)}}{r_s} - 1\right] \times 1000 \tag{3.26}$$

$$= \delta^{13}_{\mathrm{meas}} + \frac{^{13}\mathrm{C}(\tau_1) - ^{13}\mathrm{C}(\tau_2)}{^{12}\mathrm{C}(\tau_1)} \frac{1000}{r_s} \tag{3.27}$$

$$= \delta^{13}_{\mathrm{meas}} + \Delta\delta \tag{3.28}$$

where τ_1 is the effective age of ^{12}C at z, τ_2 is the effective age of ^{13}C at z, $\delta^{13}_{\mathrm{meas}}$ is the measured isotopic ratio (corrected for gravity) and r_s is the PDB standard ratio. The

correction, $\Delta\delta$, can also be written as

$$\Delta\delta = \frac{\Delta\tau \frac{d^{13}\mathrm{C}}{dt}}{^{12}\mathrm{C}(\tau_1)} \frac{1000}{r_s} \tag{3.29}$$

showing how it depends on the difference in the effective age of the two isotopes, $\Delta\tau$, and the rate of change of ^{13}C in the atmosphere. The atmospheric rate of change of ^{13}C looks very much like rate of change of CO_2, but scaled. Based on this, the diffusion correction would be expected to increase from zero at the surface to a maximum at the bottom of the firn where the age difference will be greatest. In the ice it should be largest when the corresponding rate of change of ^{13}C in the atmosphere was greatest. This expression is only particularly useful for calculating the correction when the atmospheric concentration is close to linear or exponential.

3.6.1 Model calculation of the diffusion correction for $\delta^{13}CO_2$

The following demonstrates the calculation of the diffusion correction with the model for the DE08-2 firn $\delta^{13}CO_2$ data. The firn model is run without gravitation and with three tracers:

1. Tracer 1 is $^{12}CO_2$, i.e., $^{12}CO_2$ atmospheric record and $^{12}CO_2$ diffusion coefficient, D_{12}.

2. Tracer 2 is $^{13}CO_2$, i.e., $^{13}CO_2$ atmospheric record and $^{13}CO_2$ diffusion coefficient, D_{13}.

3. Tracer 3 is forced with the $^{13}CO_2$ atmospheric record but has $^{12}CO_2$ diffusion coefficient, D_{12}.

The atmospheric records used in the model are time series of CO_2 and $^{13}CO_2$ derived from the gravitationally corrected DE08-2 firn and ice core CO_2 and $\delta^{13}CO_2$ data.

The model is used to calculate depth profiles for the three tracers, and from these, two isotopic ratio profiles are formed: (1) $\delta^{13}(D_{13})$, calculated with tracers 1 and 2 (i.e. the ^{13}C isotope is modelled with diffusion coefficient D_{13}), and (2) $\delta^{13}(D_{12})$ calculated with tracers 1 and 3. The difference between these values at each depth,

$$\Delta\delta = \delta^{13}(D_{12}) - \delta^{13}(D_{13}) \tag{3.30}$$

is used as an estimate for the diffusion correction, $\Delta\delta$. This correction reflects the difference between the value that is actually stored in the ice, $\delta^{13}(D_{13})$, and the "true" atmospheric

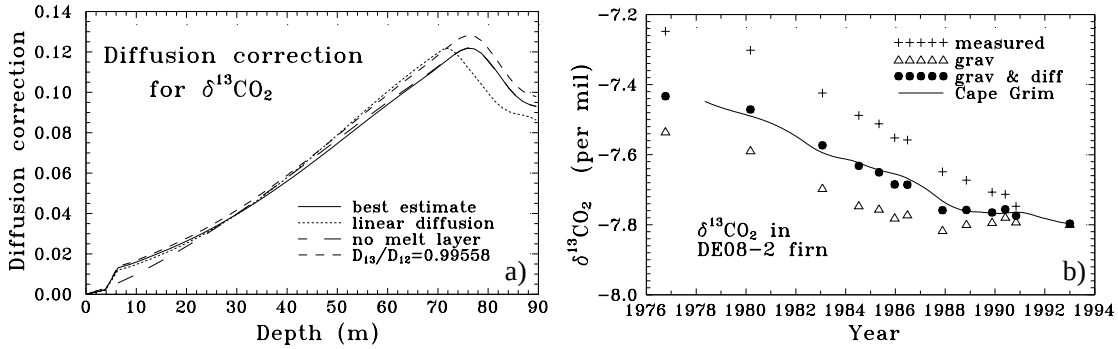

Figure 3.12: a) Diffusion correction for $\delta^{13}CO_2$ in the DE08-2 firn calculated by using the model. The solid line was calculated by using the DE08-2 diffusivity dependence, the 1990 melt layer, and $D_{13}/D_{12} = 0.9958$. Units are permil. b) Measured, gravitationally corrected (grav), and fully corrected (grav & diff) $\delta^{13}CO_2$ in the DE08-2 firn. The solid line is a spline fit to Cape Grim measurements, shifted down by 0.037‰ to allow for the spatial gradient between Law Dome and Cape Grim.

value, $\delta^{13}(D_{12})$, which is what would have been stored if the diffusion coefficients of the two isotopes were equal. Of course, $\delta^{13}(D_{12})$ is not strictly the true atmospheric value, as the diffusion and bubble trapping will have had a smoothing effect on the record. This diffusion correction is applied to the $\delta^{13}CO_2$ data to obtain a new corrected $^{13}CO_2$ atmospheric record, which is then used to repeat the calculation. On the second iteration, the diffusion correction differed by less than 0.0002‰ at any depth. Since this difference exceeds the precision of the individual measurements, the initial calculation of the correction is used in the discussion below.

Figure 3.12a shows the diffusion correction for $\delta^{13}CO_2$ in the DE08-2 firn, indicating its sensitivity to a few different assumptions. Figure 3.12b shows the measured, gravitationally corrected, and fully corrected (i.e., gravitation and diffusion) $\delta^{13}CO_2$ data for the DE08-2 firn. The firn measurements are described by Francey et al. (1999a). The gravitational correction is taken to be 0.94 times the measured DE08-2 $\delta^{15}N_2$. This value reflects the difference in the gravitational fractionation of $\delta^{13}CO_2$ compared to $\delta^{15}N_2$, which is discussed in Section 3.5.2. A spline fit to the measured $\delta^{15}N_2$ data is used rather than the actual measurements, because the precision of the $\delta^{13}CO_2$ data is greater than the precision for the $\delta^{15}N_2$ measurements for the DE08-2 firn. Also shown (solid line) is a spline fit to measurements of flask samples and archive tanks from Cape Grim. In order to allow for

spatial differences between Cape Grim and Law Dome the Cape Grim values are shifted down by 0.037‰, an amount obtained by matching the DE08 surface value to the Cape Grim value for the corresponding time. Francey et al. (1999a) discuss different estimates of the latitudinal gradient between Tasmania and the coast of Antarctica. They attribute this gradient to a ^{13}C disequilibrium flux with the oceans that varies with latitude due to the temperature dependence of the air-sea fractionation factor. The value used here is similar to the model estimates given by Francey et al.

The gravitational correction has a very large effect on the firn $\delta^{13}CO_2$ record, shifting the values near the base of the firn by around 0.3‰. The diffusion correction for $\delta^{13}CO_2$ works in the opposite direction to the gravitational correction and shifts the values about one third of the way back toward the original measurements. It is clear from this example that the diffusion correction is a critical step in the reconstruction of isotopic records from firn and ice core measurements.

Considering the large corrections involved in obtaining the firn air record, the agreement between the DE08-2 firn air $\delta^{13}CO_2$ record and the Cape Grim record is remarkable. In particular, the distinct flattening in $\delta^{13}CO_2$ observed globally in the atmosphere (Francey et al., 1995b), is evident in the firn data. It should be emphasised that the firn air results were obtained entirely independently from the Cape Grim record. The observed isotopic records were not used in calibrating the firn model or in calculating the diffusion correction. The diffusion correction for $\delta^{13}CO_2$ measurements in the ice can be calculated in exactly the same way as that for the firn, but by using the difference between the δs in the trapped air. The diffusion correction in the ice is very sensitive to the rate of change of atmospheric CO_2 (or more precisely, $^{13}CO_2$), as the rate of change determines how much the $^{13}CO_2$ value differs for a given air age difference.

In order to verify that the gravitation and diffusion corrections can be calculated separately to reconstruct $\delta^{13}C$ in the firn, the model was used in a 'full circle' calculation. A $\delta^{13}C$ atmospheric record made from the Cape Grim Air Archive data with a seasonal cycle added was used in the model to generate $\delta^{13}C$ firn data at 10m intervals. Gravitation and diffusion corrections were calculated and applied to the data as already described for the actual measurements, with good agreement, confirming the application of the corrections.

3.6.2 Diffusion correction for $\delta^{13}CH_4$

Measurements of $\delta^{13}CH_4$ in the firn or ice also require a diffusion correction, and comparison of corrected DE08-2 firn measurements with Cape Grim Air Archive measurements will provide further confirmation of the modelling. The influence of diffusion on the stable isotope ratio of methane is more dramatic than for CO_2, reflecting mainly the higher proportional difference in the mass and therefore diffusion coefficients of the two isotopes.

The diffusion correction for $\delta^{13}CH_4$ is calculated in the same way as that for $\delta^{13}CO_2$. An atmospheric record was derived from the DE08-2 firn measurements with air ages determined by using the model. This record was linearly extrapolated prior to 1980, as the model needs to be run for a few (simulated) decades before the results can be used. The rate of change of $\delta^{13}CH_4$ assumed prior to 1980 was found to have a negligible effect on the diffusion correction, as the diffusion correction is mostly determined by the rate of change of CH_4. The CH_4 record used was from Etheridge et al. (1992).

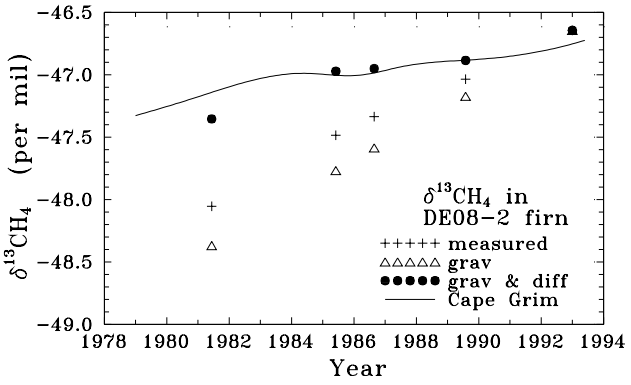

Figure 3.13: Measured, gravitationally corrected (grav), and fully corrected (grav & diff) $\delta^{13}CH_4$ for the DE08-2 firn. The solid line is a spline fit to measurements of archive tanks collected at Cape Grim.

Figure 3.13 shows the measured, gravitational corrected, and fully corrected firn values, as well as a spline fit to measurements from archive tanks collected at Cape Grim (Francey et al., 1999b). The DE08-2 surface value and the archive tank measurements have been corrected to remove the effect of seasonality by using direct atmospheric measurements from Baring Head and Scott Base (D. Lowe, pers. comm., 1995). The Baring Head and

Scott Base measurements suggest that the spatial difference between Cape Grim and DE08 is small. Overall the agreement between the firn and archive tank $\delta^{13}CH_4$ records is very good. The 1981 firn sample has slightly anomalous CH_4 concentration, which may explain the difference of the firn $\delta^{13}CH_4$ from the archive tank measurements around this time.

For both $\delta^{13}CO_2$ and $\delta^{13}CH_4$ the diffusion and gravitational corrections work in opposite directions when atmospheric concentrations are increasing. This occurs because the greater gravitational force and slower diffusion rate of the heavier isotope cause an enrichment and depletion, respectively, of the heavier isotope relative to surface ratios. The relative importance of the two corrections depends on the masses and diffusion coefficients of the two isotopes involved, as well as the atmospheric growth rates. The diffusion correction is larger than the gravitational correction for $\delta^{13}CH_4$ but not for $\delta^{13}CO_2$. Both corrections can significantly alter the apparent time rate of change of atmospheric $\delta^{13}CO_2$ and $\delta^{13}CH_4$ and are therefore very important. The agreement between the corrected isotopic firn records and direct measurements supports the method that has been used to calculate the correction for isotopic fractionation due to the diffusion process.

3.7 The Law Dome firn and ice core record

3.7.1 CO_2

The Law Dome CO_2 record from Etheridge et al. (1996) consists of ice core measurements from DE08, DE08-2 and DSS and firn measurements from DE08-2 (Figure 3.14). The firn measurements were assigned the CO_2 ages from Figure 3.8a. The uncertainty on the measurements is given by Etheridge et al. (1996) as 1.2 ppm. There are a number of features that stand out in the record, such as the strong CO_2 increase after about 1800, the decreased levels between about 1550 and 1800 and the flattening around 1940. Analysis of these features and others in terms of their biogeochemical implications will be discussed in later chapters. The focus in this section will be on how well the ice core record represents the true atmospheric history. Etheridge et al. (1996) has described aspects related to sampling and measurement. The firn model is well calibrated for DE08 and DE08-2, and confirms the age offset of 30 years determined by Etheridge et al. (1996). Less is known about DSS, as firn air composition and closed porosity measurements are not available to test model behaviour. Etheridge et al. (1996) used an age offset of 58 years for DSS.

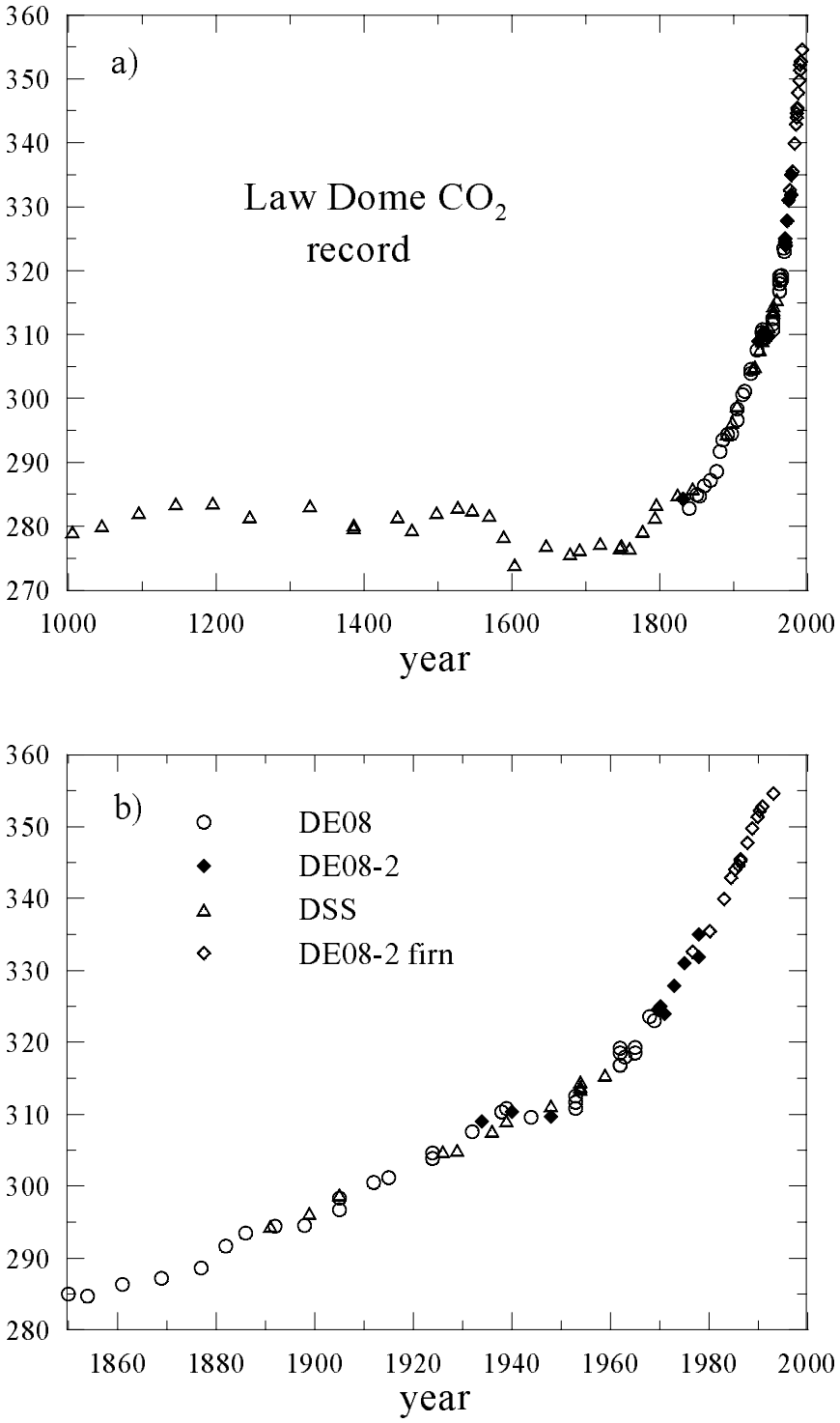

Figure 3.14: Law Dome CO_2 record (Etheridge et al., 1996) plotted over different time ranges. Measurements (in ppmv) are from DE08, DE08-2 and DSS ice cores and DE02-2 firn are shown using different symbols. The firn samples are dated with the model.

Encouragingly, there are no obvious offsets between the CO_2 records from the different cores which might have occurred if there was a problem with the dating (all cores were independently dated) or with one of the drilling techniques (different techniques were used for each of the cores).

The DE08 and DE08-2 CO_2 records show a marked flattening, or perhaps even decrease, in concentration around the 1940's (Figure 3.15a). The DSS measurements (Figure 3.14b) and the Siple and H15 measurements (Figure 3.15b) don't appear to flatten in the same way. The fact that this feature is seen at DE08 and DE08-2 but not at the other sites may be due to the different time resolutions of the sites. DE08 and DE08-2 were drilled 300 m apart, and both cores show similar flattening. The feature is unlikely to have been caused by contamination, however the possibility cannot be completely ruled out. The firn model will be used to quantify the smoothing for DE08 and DE08-2, and to see how much the atmosphere may have changed to leave such a feature trapped in the ice.

The pulse calculation in Figure 3.9a (Section 3.5.3) produced a trapped record of CO_2 that looks rather similar to the DE08 and DE08-2 measurements, although the atmospheric changes were quite extreme. Figures 3.16a and 3.16b show the results of running the firn model with a spline fit to the DE08 and DE08-2 measurements (dashed line in Figure 3.16a). The solid line in Figure 3.16b shows the calculated trapped profile versus depth and the solid line in Figure 3.16a shows this profile corrected for gravity and dated with a

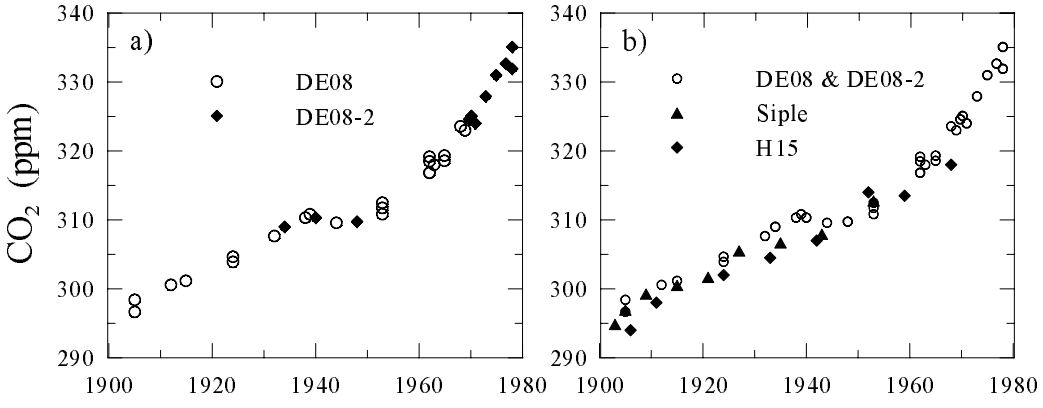

Figure 3.15: Ice core CO_2 measurements from a) DE08 and DE08-2 and b) DE08, DE08-2, Siple and H15. (See Section 2.8 for references.)

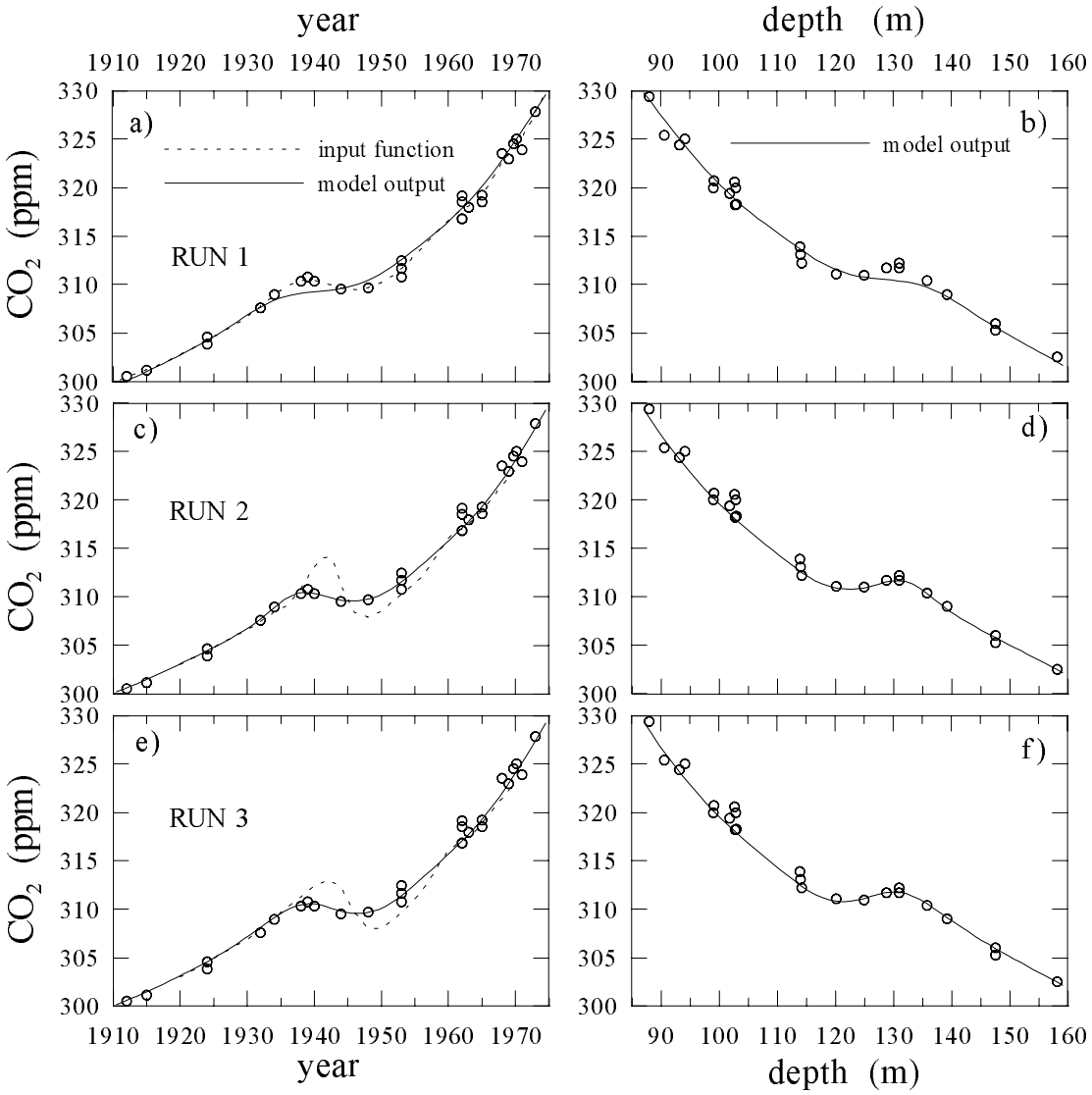

Figure 3.16: a) The solid line shows the modelled trapped concentrations for DE08-2 calculated when the dashed line is used as the atmospheric history in the firn model for DE08 and DE08-2 (RUN 1). The modelled profile is gravitationally corrected and dated with a constant age offset of 30 years. b) The same model profile plotted versus depth. The remaining plots show the same quantities for two other atmospheric histories, RUN2 (plots c) and d)) and RUN3 (e) and f)). The DE08 and DE08-2 measurements are shown in all plots, corrected for gravity in the plots on the left but not on the right. The DE08 points are plotted against 1993 depths.

constant age offset of 30 years. This calculation suggests that more extreme changes are needed to reproduce the observed concentrations. The remaining plots in Figure 3.16 show two other atmospheric records (dashed lines) that produce trapped records (solid lines) similar to the ice core measurements when run in the model. These atmospheric records were obtained by trial and error, with the aim of determining the smoothest atmospheric records that would produce output similar to the measurements.

If the model over-estimates the smoothing at DE08 and DE08-2, then smaller changes in atmospheric CO_2 than those shown in Figures 3.16c and 3.16e were probably responsible for the ice core CO_2 variations. The diffusion in the model has been well tuned to a number of different species, and should be reliable. The trapping, which can also influence smoothing for ice samples, is determined from the spline fit to DE08 porosity measurements (Figure 3.3) and this has not yet been well tested. The timing of the trapping relative to the diffusion is expected to be important for determining the degree of smoothing in the ice. The mean age of modelled trace gases in DE08 ice agrees well with the observations for simple, monotonically increasing atmospheric records. This can be seen in Figure 3.16 for CO_2 before about 1930. Probably the best way to test the smoothing for the ice is using the $^{14}CO_2$ bomb pulse. V. A. Levchenko (CSIRO AR) ran the firn diffusion model for $^{14}CO_2$ with the tuned DE08-2 diffusivity, and compared the model results with measurements of $\Delta^{14}C$ in firn and ice from DE08 and DE08-2 (Levchenko et al., 1997). Figure 3.17 shows the measured and modelled profiles from Levchenko et al. (1997), where the bands represent a range of model solutions for different ^{14}C input data and relative diffusivity values. The model does slightly under-estimate the peak in $\Delta^{14}C$ compared with the measurements, suggesting that the model may be over-smoothing. The height and shape (sharpness) of the ^{14}C bomb pulse in ice is a useful indicator of the amount of smoothing due to the firn processes, while its position in the ice gives information about effective age.

The closed porosity measurements that have been used in the model may require a significant correction for closed bubbles that are cut (and therefore appear as open porosity) when a small sample of ice is prepared (J.-M. Barnola, pers. comm., 1999). This means that the timing of trapping may not be exactly as suggested by the spline fit to the closed porosity measurements. To test the sensitivity to closed porosity, the firn model has

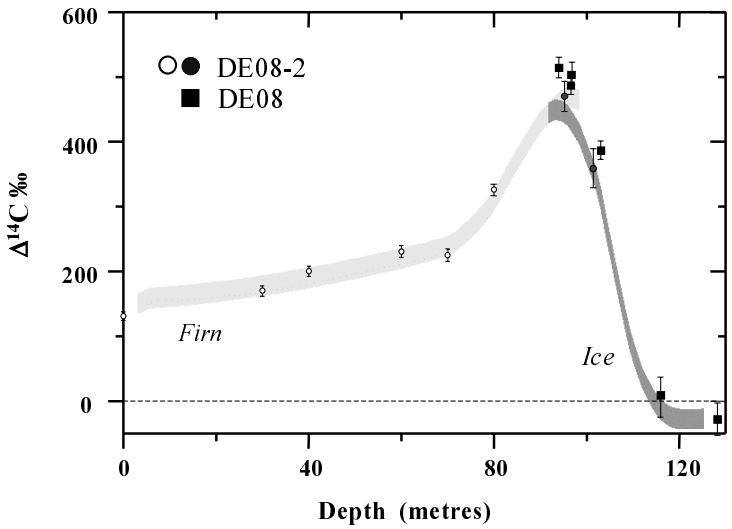

Figure 3.17: Results from Levchenko et al. (1997) using the firn diffusion model for $\Delta^{14}C$, with measurements from DE08 ice and DE08-2 firn and ice.

been run for DE08 with a number of different closed porosity curves used for trapping, but with the original porosity curve still used to determine mixing in the firn. This allows the trapping profile to change without altering the concentration profiles in the firn that have already been tuned. The different closed porosity curves for trapping made surprisingly little difference to the smoothing of the trapped concentrations. Figure 3.18a shows the standard closed porosity curve and 4 variations. The diffusivity profile versus density is also shown, and the vertical line indicates the density where diffusivity goes to zero. The modelled $\Delta^{14}C$ and CO_2 for the 5 different porosity curves are shown in Figures 3.18b and 3.18c. The 'test 1' porosity curve is based on a preliminary estimate of the influence of cut bubbles by J.-M. Barnola for Vostok (pers. comm., 1999). The 'test 3' curve gives significantly shallower trapping than the others, altering the effective age of the gas but making relatively little difference to the smoothing (as determined from the height of the ^{14}C bomb pulse). The long dashed curve in Figure 3.18c shows the concentrations in the free air (which are kept by the model even after diffusion and trapping have stopped). This is what would be stored in the trapped bubbles if all trapping occurred after diffusion had stopped. The accumulation rate at DE08 is very high, and the model calculations suggest that the smoothing of concentrations in the bubbles is not strongly affected by the closed

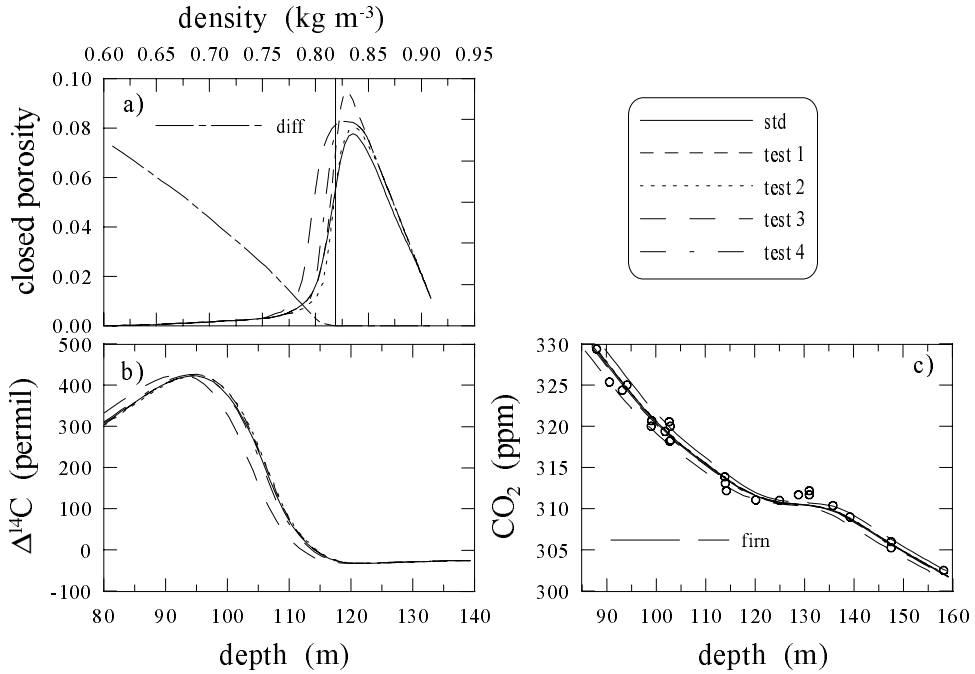

Figure 3.18: a) DE08 closed porosity versus density. The standard curve (solid line) and 4 test curves are shown, as well as the diffusivity profile. The vertical line indicates where diffusivity goes to zero. b) Trapped $\Delta^{14}C$ for DE08 modelled with the different porosity curves used to determine trapping. c) Trapped CO_2 calculated by running the spline fit to DE08 and DE08-2 CO_2 measurements with the different porosity curves. The long dashed curve shows the modelled concentration in the free air.

porosity curve. The influence of the different porosity curves on smoothing will be greater for lower accumulation rate sites.

Etheridge et al. (1996) suggested that the CO_2 stabilisation around 1940 is not seen at DSS because it has a wider air age distribution for trapped air. Compared to DE08, DSS has a lower accumulation rate, so the smoothing due to trapping would be expected to be greater at DSS than DE08. However, DSS has a shallower sealing depth than DE08 (density increases more rapidly with depth), which should give less smoothing due to diffusion at DSS. Quantifying the smoothing at DSS is difficult without firn measurements to validate the modelling, but we can use the model to test a range of possibilities. Figure 3.19 shows the modelled age distributions for CO_2 trapped in ice at DE08 and DSS, where the model run for DSS uses DSS density, DE08 open porosity and DE08-2 tuned diffusivity. The two sites have similar temperatures, fairly high accumulation rates and

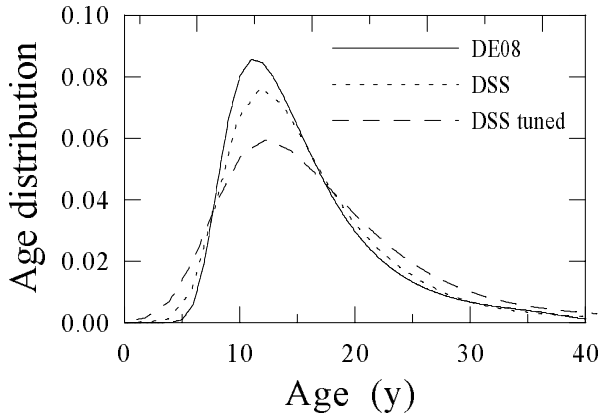

Figure 3.19: Age distribution of CO_2 trapped in the ice at DE08 and DSS. The DSS model run used a fit to DSS density measurements, DE08 closed porosity and the DE08-2 tuned diffusivity. The DSS tuned run used DSS97 density, DE08 closed porosity and DSS tuned diffusivity. The DSS and DSS tuned curves have been shifted by 15.7 and 17.7 years, respectively, so that the peaks roughly coincide, to help visual comparison.

are located fairly close to each other, so the assumption that the diffusion and porosity is similar is not unreasonable. The calculated age distribution for DSS is wider than for DE08, but not a great deal.

Figure 3.20 shows the trapped CO_2 concentrations around 1940 calculated for DSS using the same atmospheric records as in Figure 3.16. The effect of the lower accumulation rate, offset slightly by the shorter firn column, is not enough to explain the absence of flattening in CO_2 at DSS. The model again suggests only a small difference in smoothing between DSS and DE08.

The bomb pulse in $\Delta^{14}CO_2$ has been measured in DSS ice and should provide a good opportunity to test the smoothing at DSS. Figure 3.21 shows the DSS $\Delta^{14}C$ measurements from Levchenko et al. (in prep.). For these measurements, it was not always possible to avoid using summer ice, so the samples may contain some air that is younger and less smoothed than from the non-summer ice. Different symbols in Figure 3.21 distinguish measurements of air extracted from samples consisting partly of summer ice and containing no summer ice, as summer ice is believed to contain younger air. $\Delta^{14}C$ calculated with the firn model using the standard DSS inputs (DSS density, DE08 porosity and diffusivity) is shown by the solid line. The deepest $\Delta^{14}C$ measurements are clearly elevated relative to pre-bomb levels. This excess ^{14}C is likely to have been caused by ^{14}C produced *in*

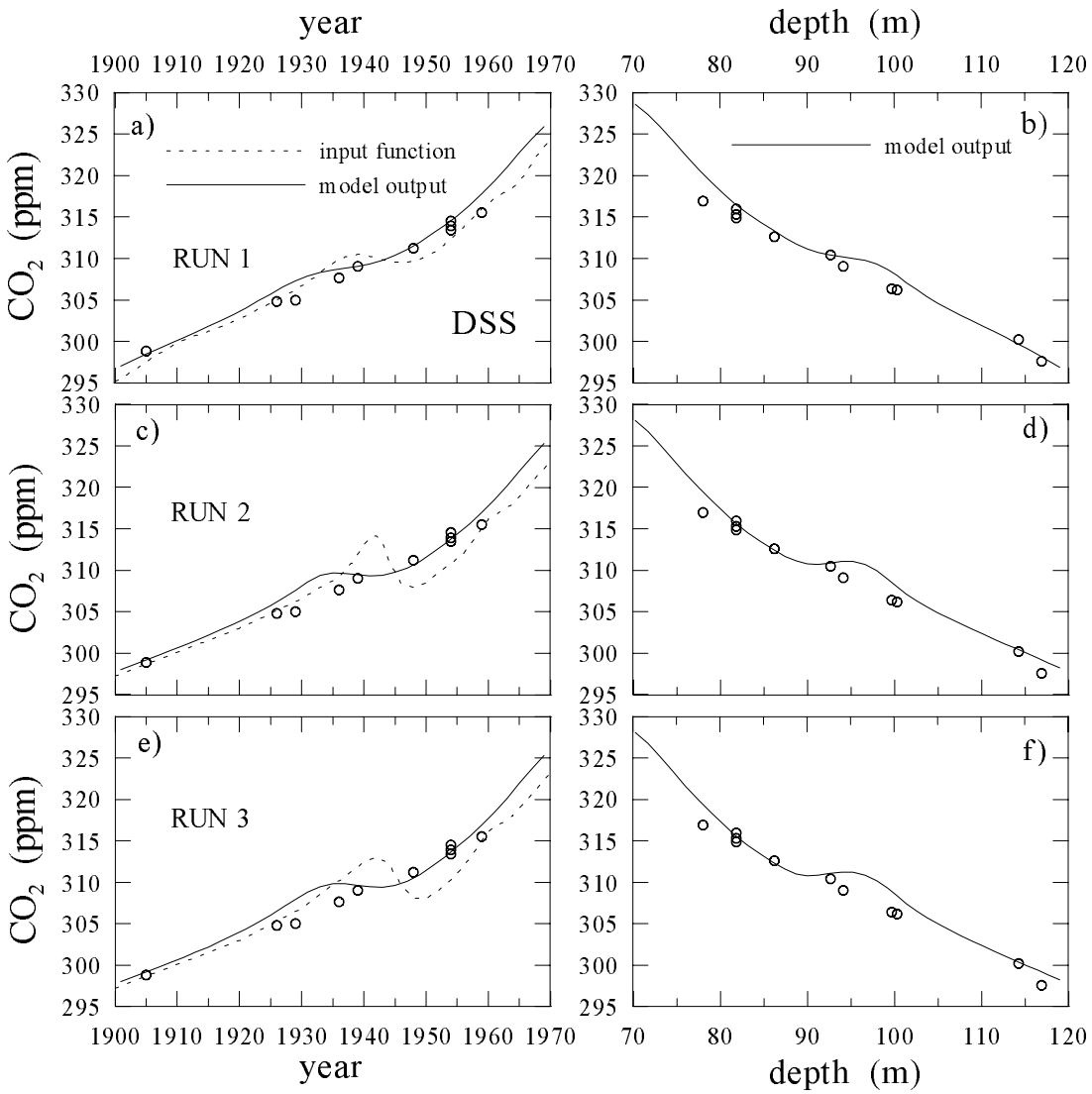

Figure 3.20: Modelled trapped concentrations for DSS calculated with the same atmospheric inputs as in Figure 3.16. The model is run with DSS density, DE08 porosity and DE08-2 tuned diffusivity. The dashed lines show the atmospheric inputs, the solid lines on the left are the calculated concentrations dated with an age offset of 58 years and gravitationally corrected, and the solid lines on the right are the calculated concentrations versus depth. Observations are from Etheridge et al. (1996).

situ in the ice when the ice was near the surface (Smith et al., 2000). The amount of ^{14}C produced *in situ* in the ice at DSS was predicted by V. Levchenko (CSIRO AR). The degree of transfer of ^{14}C between the ice and air bubbles is not known. The grey symbols in Figure 3.21 show the $\Delta^{14}C$ measurements after subtracting the estimated *in situ* component from all measurements. This correction assumes that all of the *in situ* produced ^{14}C has escaped from the ice into the air bubbles, either before or after drilling. V. Levchenko tuned the diffusivity and accumulation rate for DSS to try to give the best fit to the corrected $\Delta^{14}C$ measurements. None of the combinations tried were able to reduce the modelled peak to the level of the corrected measurements at the top of the peak, while still fitting the two measurements around 80 m. Smith et al. (2000) have speculated on the reason for this. They suggest that the deeper samples contain *in situ*

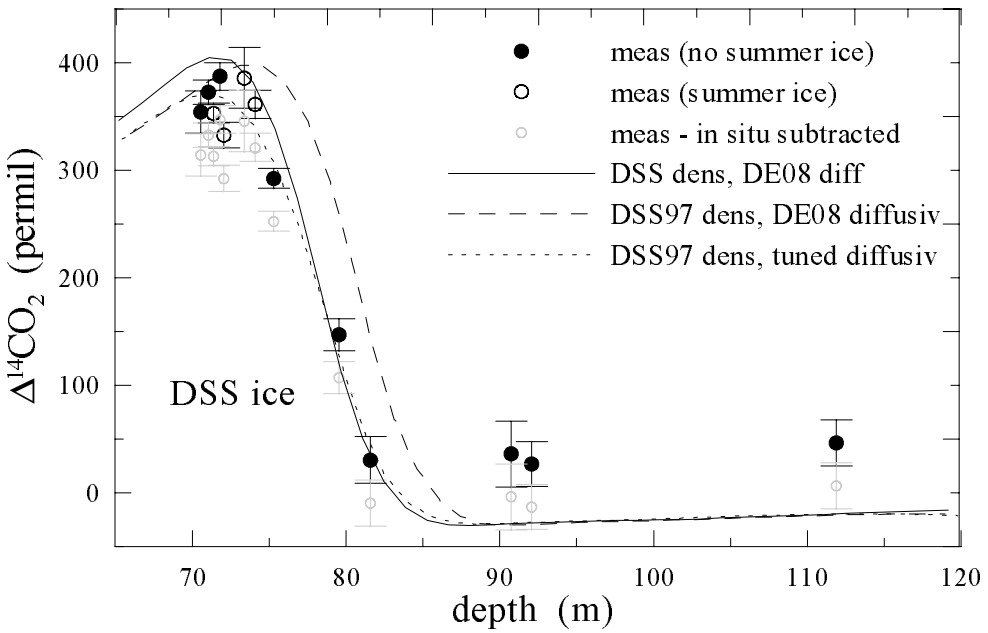

Figure 3.21: $\Delta^{14}CO_2$ in DSS ice. Measurements from Levchenko et al. (in prep.) are indicated by the solid circles when no summer ice was used and open circles when the sample was partly from summer ice. The grey circles show these measurements after subtracting the estimated contribution due to *in situ* production of 52 ‰ (Smith et al., 2000). The solid line shows the modelled $\Delta^{14}C$ calculated with the original DSS density profile and DE08 porosity and diffusivity. The dashed line is modelled with the DSS97 density and the DE08 porosity and diffusivity. The dotted line used DSS97 density, DE08 porosity and diffusivity tuned to give the best fit to the uncorrected $\Delta^{14}C$ measurements. Model calculations were run by V. Levchenko (CSIRO AR).

produced ^{14}C, but that the shallower samples do not. This may be due to some process that takes time to release the ^{14}C from the ice, or perhaps that the air pressure in the deeper air bubbles is very high, and relaxation of pressure after drilling causes the excess ^{14}C in the ice to get into the bubbles. The pressure in the shallower samples is closer to atmospheric, so relaxation is not significant. Measurements of $\Delta^{14}C$ from air bubbles in DE08 and DSSW20K ice showed no evidence of *in situ* produced ^{14}C (V. Levchenko, pers. comm.). At DE08 the expected *in situ* production is small due to the high accumulation rate. The DSSW20K ice spent only a short time in storage before extraction of air and analysis, perhaps not long enough for the relaxation and exchange to occur (Smith et al., 2000). These explanations are speculative, and at present the uncertainties are quite high. Further measurement of $\Delta^{14}C$ at different sites, depths and times after drilling should be able to improve understanding of these processes.

The firn model calculations by V. Levchenko used a density profile fitted to the DSS and DSS97 density measurements (unpublished data from the Australian Antarctic Division) shown in Figure 3.22a. The calculated $\Delta^{14}C$ with this density and DE08 porosity and diffusivity is shown by the dashed line in Figure 3.21. The bomb pulse is trapped deeper in the ice due to the slightly longer firn column for this density profile. The best fit of modelled $\Delta^{14}C$ to the uncorrected ice core measurements using the DSS97 density, DE08 porosity, tuned diffusivity and an accumulation rate of 570 kg m^{-2} yr^{-1} is shown by the dotted line in Figure 3.21. The $\Delta^{14}C$ peak is reduced and smoothing increased compared to the DE08 diffusivity runs. Levchenko et al. (in prep) describe a method to quantify the smoothing calculated by the firn model. The concentration profile with depth is calculated with the model for a linear and quadratically increasing tracer. The linear tracer gives the mean age as already described. By combining the results for the two tracers they estimate the mean square deviation of ages at each depth in the firn and ice, and take this as a measure of the age spread. The range of solutions that give reasonable agreement with the measured $\Delta^{14}C$ at DSS all have smoothing in the range 18–20 years. This is compared with the model estimate of 11.5 years for DE08 (V. Levchenko, pers. comm.).

The CO_2 pulse calculations with the RUN1 atmospheric inputs were performed for DSS using the tuned diffusivity. These are shown in Figure 3.23. The smoothing on the CO_2 feature is increased in both cases compared with the previous DSS runs, but the

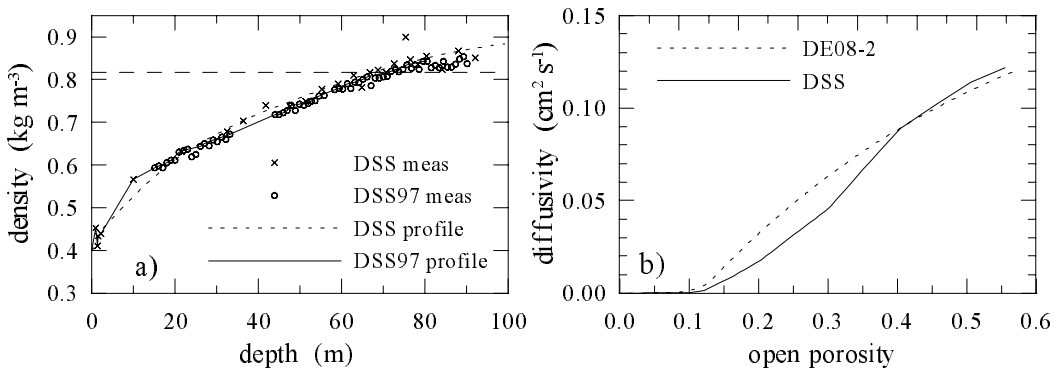

Figure 3.22: a) DSS and DSS97 density measurements (unpublished data from the Australian Antarctic Division) and the DSS and DSS97 density profiles used in the firn model. The dashed line shows the density that diffusivity goes to zero for the DE08-2 diffusivity. b) Diffusivity tuned by V. Levchenko (CSIRO AR) to give the best match to DSS Δ^{14}C measurements (solid line). The dotted line shows the DE08-2 diffusivity.

RUN3 case still suggests more variation than is seen in the measurements.

There are a number of uncertainties in modelling DSS. The ice properties density, porosity, diffusivity and the accumulation rate are known approximately but the uncertainties in these quantities lead to significant uncertainties in the calculated trace gas profiles. The lack of concentration data from the firn at DSS is a real disadvantage. The best information on DSS comes from Δ^{14}C, but the large uncertainties in the *in situ* ^{14}C

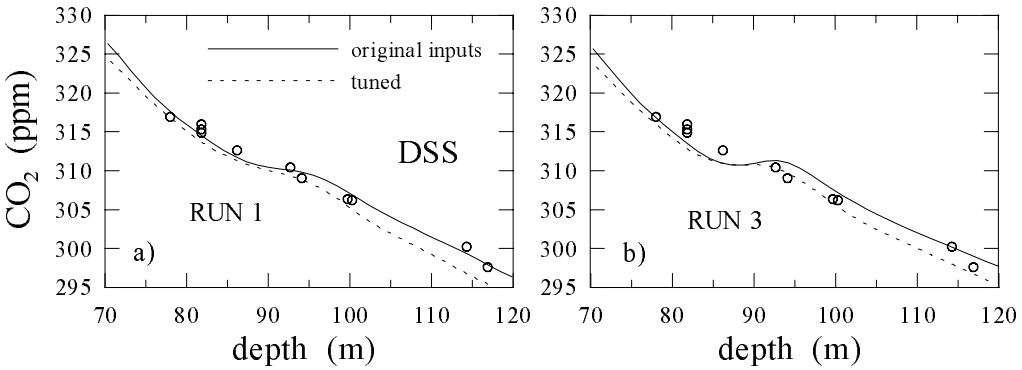

Figure 3.23: a) Modelled trapped CO_2 for RUN1 atmospheric input for the original DSS inputs (DSS density, DE98 porosity and diffusivity) and for tuned inputs (DSS97 density, DE08 porosity and tuned diffusivity). b) The same model runs for RUN3 atmospheric input.

production really need to be resolved before $\Delta^{14}C$ can be used to conclusively quantify smoothing. If an *in situ* production correction is required for the measurements, either part of or all of that suggested by V. Levchenko, then this would reduce the trapped $\Delta^{14}C$ peak and imply that the smoothing at DSS is greater than currently predicted. This would likely explain the absence of the CO_2 flattening in DSS ice. It is not clear, however, how reduced smoothing at DSS could be achieved in the model.

In summary, the actual CO_2 variation around the 1940s was probably somewhere between the RUN1 and RUN3 curves shown in Figure 3.16, close to RUN3 if the model smoothing for DE08 is correct or closer to RUN1 if it over-estimates smoothing. The lack of CO_2 feature at DSS can be explained by the greater smoothing, as suggested by Etheridge et al. (1996). The small mismatch between DE08/DE08-2 $\Delta^{14}C$ measurements and the modelled profile is not on its own seen as grounds to retune the model for DE08. Diffusivity in the firn has been tuned to give an excellent match to a number of tracers, and agrees well with firn $\Delta^{14}C$. The trapping distribution has been shown to make only a small difference to smoothing of the bomb pulse and the CO_2 pulse.

3.7.2 $\delta^{13}CO_2$

The Law Dome $\delta^{13}CO_2$ record (Francey et al., 1999a) is shown in Figure 3.24. There are a number of corrections that had to be applied to the raw measurements to get this record, and these are detailed in Francey et al. (1999a). They include a number of corrections associated with extraction and measurement, as well as the correction for gravitational fractionation and the diffusion correction. The gravitational correction was determined with the firn model, as the only measurements of $\delta^{15}N_2$ in the ice were preliminary and quite scattered. The model gives a value of 0.26 ‰ for gravitational fractionation for $\delta^{13}C$ at both DE08 (with DE08 inputs) and DSS (with DSS density and DE08 porosity and diffusivity).

The diffusion correction was also determined with the model. Figure 3.25 shows the diffusion correction for the DSS ice core. Also shown is the growth rate of CO_2 in the atmosphere determined from the Law Dome CO_2 record (this is the derivative of the concentration record that is used in calculating the diffusion correction). As expected from Equation 3.29, the diffusion correction very closely follows the CO_2 gradient, but smoothed by the firn processes. The ratio of the diffusion correction to the CO_2 growth

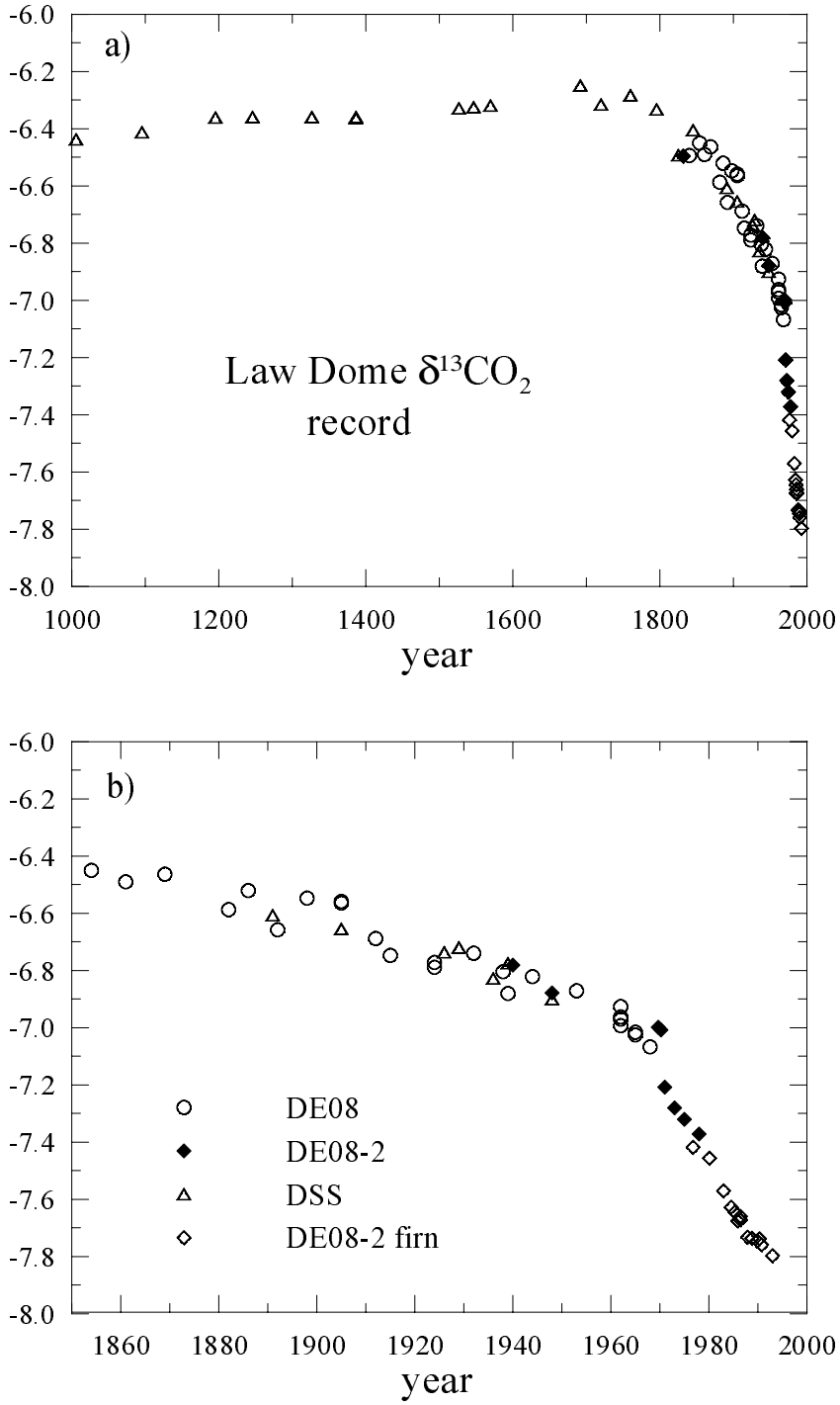

Figure 3.24: Law Dome $\delta^{13}CO_2$ record (Francey et al., 1999a) plotted over different time ranges. Measurements (in permil) from DE08, DE08-2 and DSS ice cores and DE02-2 firn are shown using different symbols. The firn samples are dated with the model.

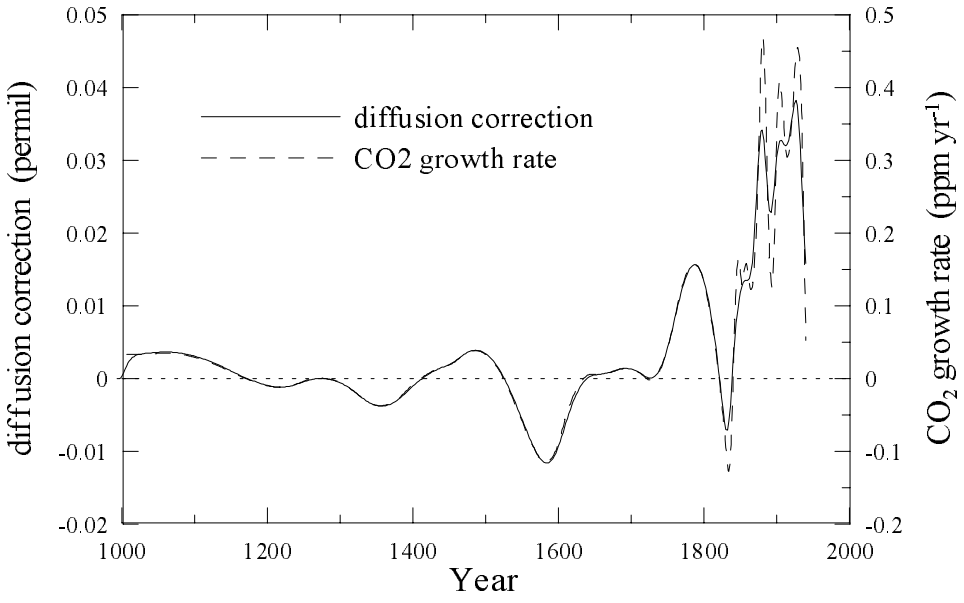

Figure 3.25: Diffusion correction for DSS calculated with the model. The dashed line shows the growth rate of CO_2 from the Law Dome ice core record.

rate is very close to 0.1 for DSS, but is different for other cores depending on the effective ages at the bottom of the firn. The diffusion correction was also calculated for DSS with 2 different spline fits to the CO_2 record, as shown in Figure 3.26. This gives an indication of the uncertainty on the diffusion correction. The diffusion correction over the pre-industrial period is a very small correction compared with the uncertainty on the measurements and the other corrections.

Francey et al. (1999a) gave uncertainties of 0.025 ‰ for most of the $\delta^{13}C$ measurements, however some measurements were assigned higher errors as they had evidence of ethanol contamination but still 2 or 3 acceptable sample reference comparisons. A number of samples were rejected due to the ethanol contamination. There are two $\delta^{13}C$ measurements (1969.7 and 1970.2) that were considered outliers by Francey et al. (1999a). They were the only DE08-2 samples analysed in 1995 (the others were done in 1993) and they are considerably higher than the surrounding points. There was no evidence of a difference between samples measured in 1993 and 1995 for the DE08 and DSS cores and the reason for the high values in the two DE08-2 samples is not known. Francey et al. (1999a) estimated the uncertainties on the ice core versus firn measurements as < 0.03 ‰ and the

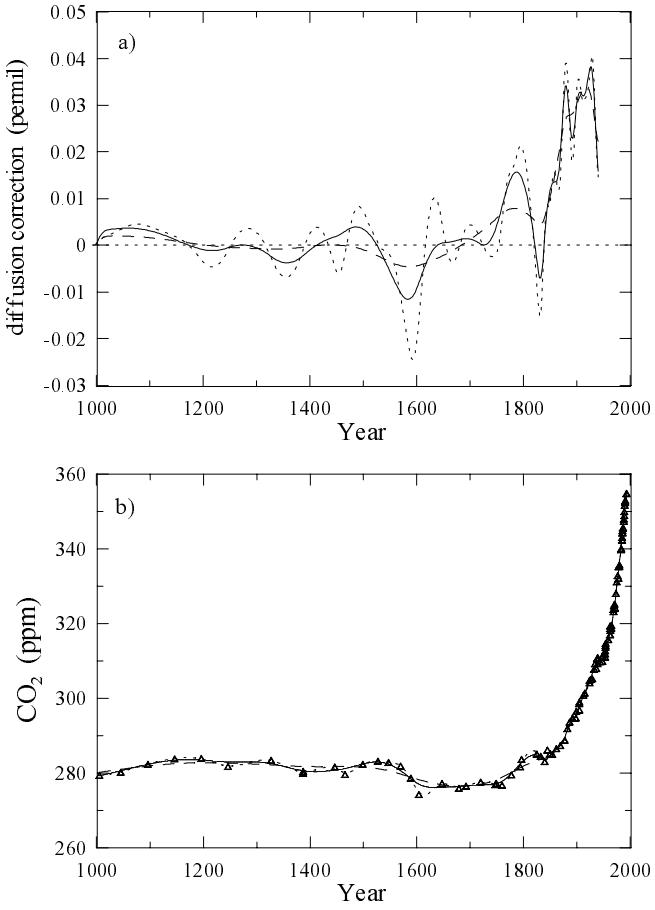

Figure 3.26: a) Diffusion correction for DSS calculated with 3 different CO_2 spline fits to the Law Dome CO_2 record. Splines are shown in b) with the same line types.

uncertainties on the Law Dome measurements relative to the troposphere as < 0.03 ‰. The gravitational correction and the blank correction (for the effect of air and CO_2 extraction) contribute most to the uncertainty on ice core versus firn measurements. Francey et al. (1999a) pointed out that the overlap between firn and ice measurements shows no obvious offset.

During the LIA period, when CO_2 was low, the Law Dome ice core record shows high levels of $\delta^{13}C$. Thermal fractionation effects, which are important for large changes in temperature such as during the glacial–interglacial transitions, are expected to have been negligible for the small temperature changes associated with the LIA.

Around the 1940s, when there is a clear flattening in the DE08 and DE08-2 CO_2 record, the $\delta^{13}C$ shows no clear feature that seems to correspond to the CO_2. Figure 3.27

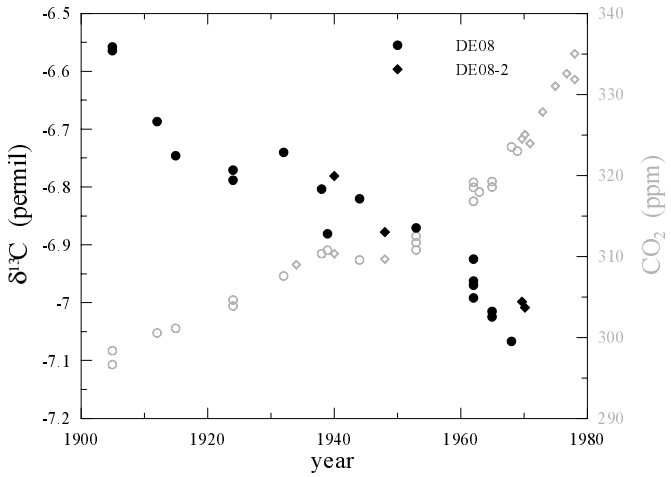

Figure 3.27: DE08 and DE08-2 δ^{13}C ice core measurements. The CO_2 measurements from these sites are shown in grey.

shows just the DE08 and DE08-2 δ^{13}C measurements through this period, with the CO_2 measurements in grey. The δ^{13}C measurements are perhaps a bit too scattered to draw firm conclusions about the δ^{13}C variation at this time.

Variations in the CO_2 growth rate can cause features in δ^{13}C in air trapped in ice even when atmospheric δ^{13}C remains constant or changes linearly. The diffusion correction is designed to correct for this, but if the 'true' atmospheric CO_2 history is not known exactly (which is generally the case), the features due to CO_2 variations will not be totally removed. Figure 3.28a shows the diffusion correction for DE08 calculated with a very smooth CO_2 spline (dashed line) and with the RUN3 CO_2 history from the previous section (solid line). The δ^{13}C input used in both cases is a smooth spline fit to the fully corrected Law Dome δ^{13}C record. Figure 3.28b shows the DE08 and DE08-2 δ^{13}C measurements corrected with each of these diffusion corrections instead of the standard one used in Francey et al. (1999a). The difference between the two diffusion corrections is much smaller than the scatter in the δ^{13}C measurements, so this effect is presently not very important. However it will become more important as measurement precision improves. Figure 3.28c shows the input δ^{13}C curve (solid line), the trapped δ^{13}C profile calculated with the RUN3 CO_2 curve and dated as in the previous section (dashed line) and the calculated profile plus the calculated diffusion correction (dotted line). In this case the 'bump' in δ^{13}C around 1940 introduced into the δ^{13}C ice core record by the CO_2 feature is removed by the diffusion

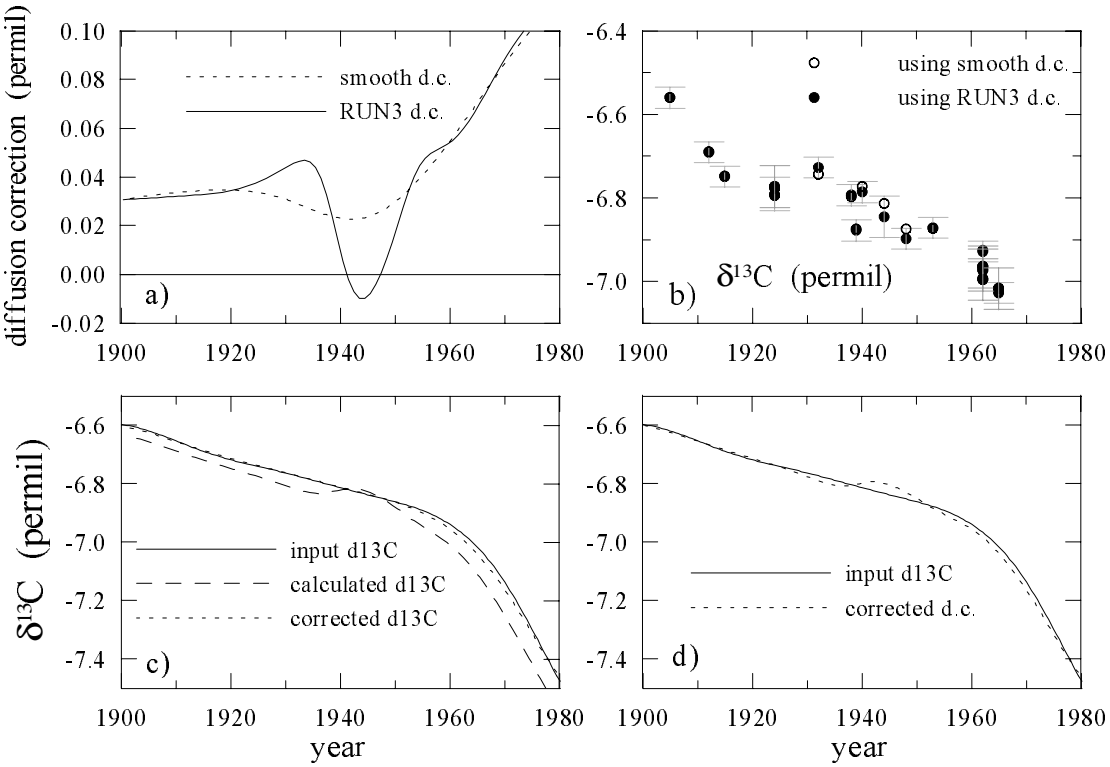

Figure 3.28: a) Diffusion correction for DE08 δ^{13}C calculated with the RUN3 CO_2 record from Section 3.7.1 and a smooth spline fit to the CO_2 ice core record. b) DE08 and DE08-2 δ^{13}C ice core measurements with the corrections shown in a). The uncertainties estimated by Francey et al. (1999a) are also shown. c) The solid line shows the input δ^{13}C atmospheric history, the longer dashes the (dated) δ^{13}C profile calculated for this δ^{13}C input and the RUN3 CO_2 input, and the calculated profile corrected with the calculated diffusion correction. d) δ^{13}C input and the profile calculated with the RUN3 CO_2 history but corrected using the diffusion correction calculated with the smooth CO_2 curve.

correction. Figure 3.28d shows the δ^{13}C input and the δ^{13}C calculated with the RUN3 CO_2 curve but corrected with the diffusion correction determined with the standard CO_2 input. Now the reconstructed δ^{13}C shows a feature that is due to the atmospheric CO_2 variations, not δ^{13}C variations. The change in the slope of the atmospheric δ^{13}C decrease that occurs after about 1955 is smoothed slightly in the trapped record compared to the input (dotted and solid lines in Figure 3.28c). This suggests that the actual change in slope in the atmosphere may have been sharper than in the Law Dome δ^{13}C record. A 'full circle' type calculation for trapped air, similar to that for the firn described in Section 3.6.1 confirms the separate application of the gravitational and diffusion corrections.

3.8 Firn $\delta^{13}CO_2$ records

Ice core records at high accumulation rate sites such as those on Law Dome offer the best way to get high time resolution records of CO_2 and $\delta^{13}C$. It is useful, however, to have a way of checking these records. Extraction of air from ice and our understanding of the bubble trapping can be tested by comparing with firn records at sites where firn air dates back many decades. This is particularly important for $\delta^{13}C$, because there are some uncertainties in the ice core measurements (Francey et al., 1999a). There is considerable loss of time resolution in the long firn records compared with the Law Dome ice core record because the long firn records are typically from low accumulation rate sites. However, they are useful because they don't involve extraction of air from ice.

Battle et al. (1996) collected firn air from South Pole in January 1995. In this section, South Pole measurements are used to reconstruct atmospheric $\delta^{13}C$ levels for comparison with the Law Dome $\delta^{13}C$ ice core record. This requires calculation of the diffusion correction and effective ages for the firn samples, and as these are both best done with the firn model, the model must first be calibrated for the site. Density was measured at South Pole, but not open porosity. Rather than impose an open porosity profile from a different site, diffusivity is specified as a function of density, and tuned to give the best fit to the CO_2 and CH_4 measurements at South Pole. The variation in open porosity through the firn would be needed to calculate trapped concentrations, but is not necessary for firn concentrations. Figure 3.29 shows South Pole CO_2, CH_4 and $\delta^{15}N_2$ firn measurements and model calculations for the tuned diffusivity profile. As for DE08-2, diffusivity was tuned by trial and error. The relative diffusion coefficient for CH_4 used in this calculation was 1.42 rather than the 1.29 given in Section 3.4.2. The value of 1.29 gave concentrations that were low compared to the measurements throughout the firn, while 1.42 was chosen to give a good fit. Model studies by other authors have used different relative diffusion coefficients for CH_4 (e.g., 1.415 by Arnaud (1997) and Rommelaere et al. (1997); 1.35 by Schwander et al. (1993) and Battle et al., (1996)). Equation 3.16 gives a value of 1.4. The model applies the correction for pressure and temperature to the relative diffusion coefficients in Table 3.2 as explained in Section 3.4.2, but this gives only small variation for different sites (the relative coefficient for CH_4 is 1.2913 and 1.2856 for DE08 and South Pole site parameters, respectively). The uncertainty in this value really needs to be resolved, but

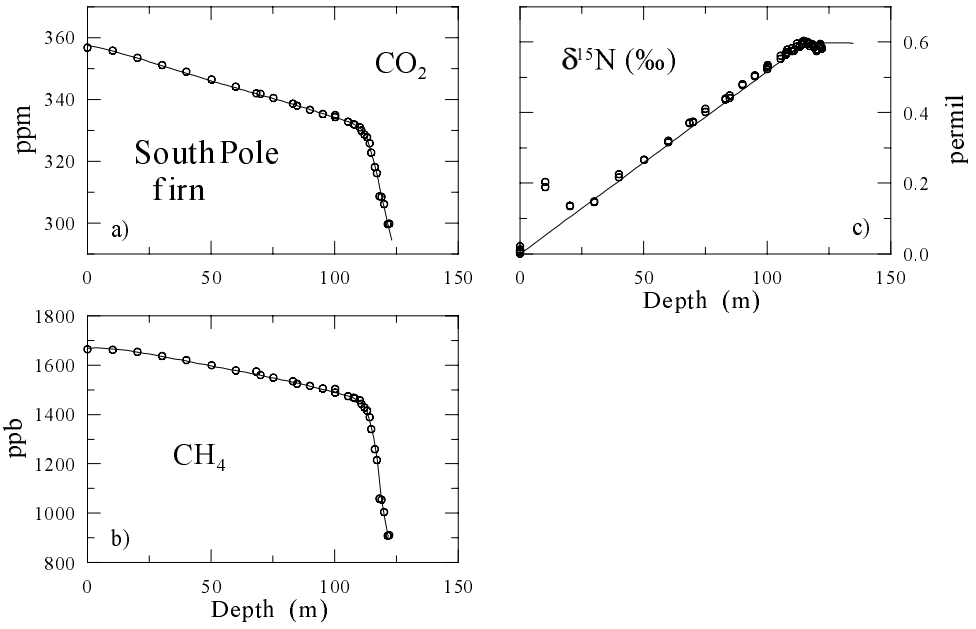

Figure 3.29: Modelled trace gases in the South Pole firn. Measurements are from Battle et al. (1996).

doesn't alter the conclusions here.

The South Pole δ^{13}C measurements are assigned CO_2 dates estimated by the model, so it is important that the model accurately match CO_2 versus depth. An alternative dating method is to assign CO_2 ages by direct comparison of CO_2 firn measurements with a spline fit to the Law Dome ice core record, without use of the firn model. If the model is well tuned the two dating methods are quite similar, except that dating with the model is slightly superior to direct comparison for the following reason. The model is used to assign a date to each depth in the firn, using a (fairly smooth) spline fit to the Law Dome ice core record. This results in a smooth, monotonically increasing age versus depth profile that is consistent with the atmospheric CO_2 variations. Direct comparison with the ice core record dates each firn measurement based on its concentration. If there is some scatter in the firn measurements this may lead to an age versus depth profile that does not increase smoothly and monotonically. If there are two measurements from the same depth in the firn with different concentration values, dating with the model would give them the same age, whereas dating by direct comparison would give them different ages. For the two corresponding δ^{13}C measurements, it would be better to give them the same age, and

accept that there is scatter, than to treat them as two measurements with different ages. In addition, dating directly from the Law Dome CO_2 ice core record is ambiguous around 1940 because the atmospheric CO_2 growth rate drops to zero.

Figure 3.30a shows the South Pole CO_2 measurements corrected for gravity and dated with a CO_2 spline in the model. The excellent agreement with the Law Dome ice core measurements confirms the calibration of the diffusivity, as this is a more sensitive test than the concentration profile versus depth. The sample from 117.99 m in the South Pole firn (CO_2 age of 1940.9) is lower than the Law Dome measurements for this time. As it is around the time of the flattening, dating will be a bit ambiguous. Apart from that, this value sits lower than the modelled CO_2 profile in Figure 3.29a. This could just be a low measurement, or could reflect an error in the CO_2 input function that was used in tuning diffusivity.

The $\delta^{13}C$ diffusion correction is calculated with the model as already described. Figure 3.30b shows the South Pole firn $\delta^{13}C$ measurements, dated and corrected for gravity and diffusion. These are compared with the Law Dome measurements. The South Pole measurements after about 1970 agree well with the Law Dome record, but before 1970 they are significantly lower. The sample dated 1940.9 should perhaps be ignored, because the difference in CO_2 for this sample has not been explained, and as it is around the CO_2 flattening, dating will be a problem. For the other measurements, the difference between the South Pole and Law Dome $\delta^{13}C$ increases with depth in the ice (and age of the air). M. Battle and M. Bender (Princeton Uni.) also see this discrepancy in their analysis of the South Pole measurements using a different firn model and dating South Pole directly from the Law Dome record. The reasons for this difference are not known, and it could be either the firn or ice core measurements (or both) that are in error.

The shallowest Law Dome ice sample has a CO_2 age of 1978. There could be a number of possible explanations for an error in the Law Dome ice core measurements relative to the Law Dome firn measurements (e.g. due to the different techniques involved in extraction of air from ice compared to pumping air from firn) but this is not how the discrepancy appears, as South Pole measurements agree with Law Dome ice measurements through most of the 1970s and with Law Dome firn measurements after that. At South Pole, diffusion stops at a depth corresponding to a CO_2 age in the early 1970s. The difference

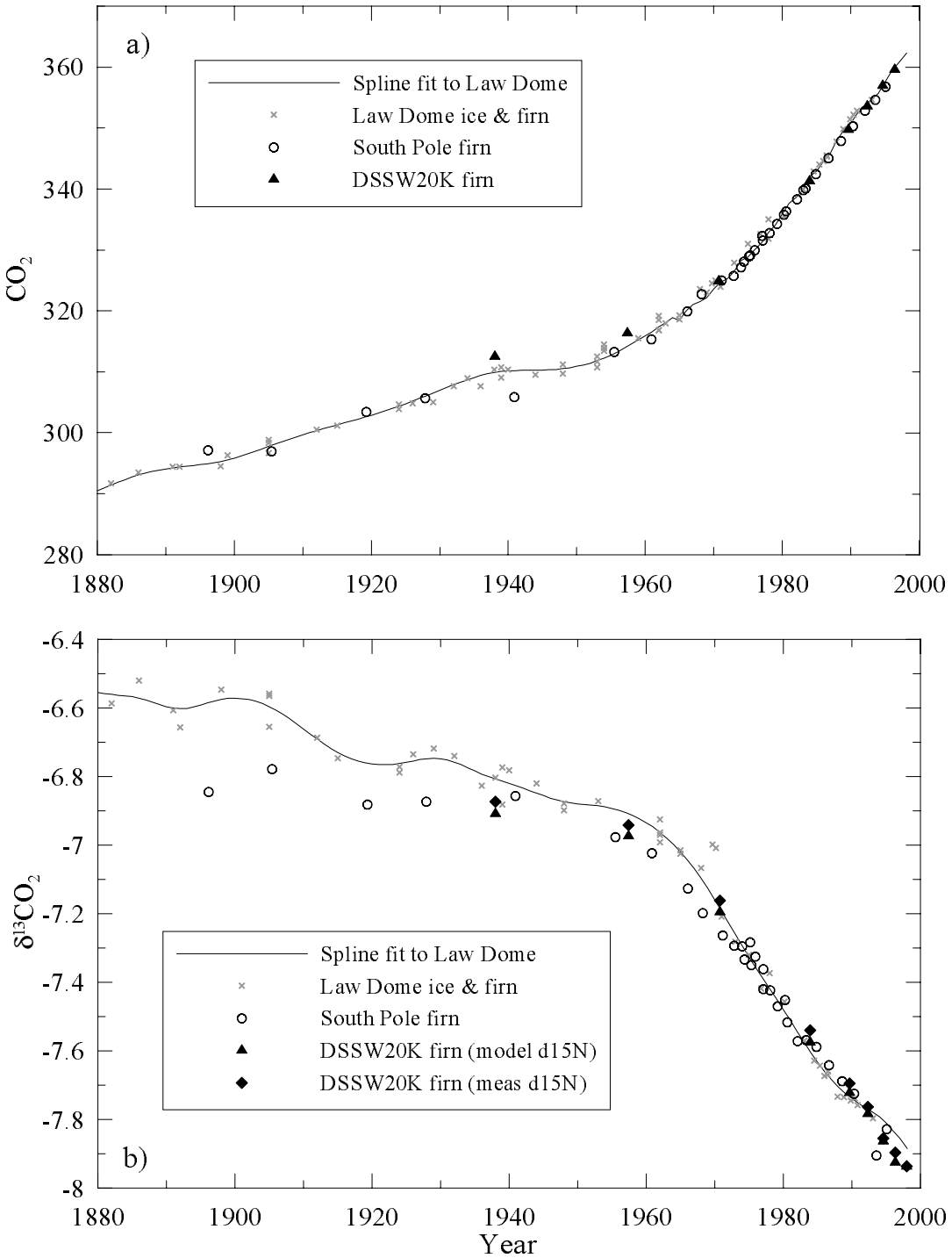

Figure 3.30: a) CO_2 from South Pole and DSSW20K firn dated with the firn model, compared with the Law Dome ice core record. b) Comparison of South Pole and DSSW20K $\delta^{13}CO_2$ firn records and Law Dome ice core record.

of South Pole from Law Dome increases with depth through the non-diffusive part of the South Pole firn.

It is difficult to identify a process that might explain a difference as big as that observed (greater than 0.1 ‰ for the lowest four South Pole samples and greater than 0.2 ‰ for the lowest) and that increases with depth / air age. The diffusion correction for the South Pole firn measurements has a maximum of about 0.26 ‰ corresponding to a date of 1973. The gravitational correction is large (0.26 ‰ for Law Dome ice and 0.6 ‰ for South Pole firn after diffusion has stopped), but a fairly constant value has been used for both firn and ice δ^{13}C measurements with dates before 1970.

The following is a list of some of the possible causes of this discrepancy, based on discussions with D. Etheridge and R. Francey (CSIRO AR) and M. Battle and M. Bender (Princeton Uni.). Possible reasons why the Law Dome ice core measurements could be in error, assuming that the South Pole firn measurements are correct are:

- Error in the gravitational correction due to barriers to mixing or variations in accumulation rate or temperature. This is **extremely unlikely** because a trend with depth is required. There is no structural evidence for this, and δ^{13}C records from DE08, DE08-2 and DSS with different site characteristics agree.

- Error in the diffusion correction. This is **extremely unlikely** because a trend is required. The diffusion correction is less than 0.04 ‰ before 1950, and rises to just over 0.1 ‰ for the shallowest ice core measurements. The diffusion correction would need to be of the wrong sign for Law Dome to agree with South Pole before 1950. The diffusion correction has been well checked for $\delta^{13}CH_4$ and $\delta^{13}CO_2$ in the DE08-2 firn.

- Exchange of air between air bubbles and ice, with organic impurities in the ice (such as in Greenland ice). This is **unlikely**, because there is no evidence of large concentrations of organic impurities in Antarctic ice, and even if there was, it would cause a depletion of ^{13}C, whereas an enrichment is measured. There is no evidence of significant carbonate impurities in the ice. If contamination with modern air had occurred, it would have decreased the δ^{13}C, so cannot explain an increase relative to South Pole.

- Measurement error. Measurement errors have been discussed extensively by Francey et al. (1999a). The only identified influence which could have a depth dependence (apart from gravity and diffusion discussed above) is the sample size correction. This correction is potentially more important for deeper samples, but is offset in that the $\delta^{13}C$ difference from the standard was small for deeper samples. No significant depth dependence is apparent in the measurements, making this explanation **unlikely**.

Possible reasons why the South Pole firn measurements could be in error, assuming that the Law Dome ice core measurements are correct, are:

- Error in the gravitational correction. This is **extremely unlikely**, as modelled $\delta^{15}N_2$ agrees with well with measurements. Even though the gravitational correction is large, it is fairly constant after diffusion stops (at a depth with a CO_2 age in the early 1970s). The discrepancy with the Law Dome record increases with depth through the non-diffusive part of the firn, and there is no reason to expect the effect of gravity to be substantially lower for deeper samples.

- Error in the diffusion correction. This is **unlikely**. The South Pole diffusion correction has a maximum of about 0.26 ‰ corresponding to a date of 1973, and decreases rapidly with depth below that (as the CO_2 growth rate decreases going back in time). The diffusion correction would need to increase with depth for samples prior to 1950 to give agreement between South Pole and Law Dome, and this is not expected. The diffusion correction was also calculated by M. Battle, with a different model that was independently tuned for South Pole, with very similar results.

- Sampling. Systematic influence, such as mass dependent fractionation from pumping through constrained pores is **unlikely** because the other tracers and isotopes show no evidence of this. A CO_2-specific effect, such as contamination from polymer surfaces when pumping deep samples at low pressure **cannot be excluded** with the available information.

- Measurement. A measurement error due to undersized samples is **unlikely**, as sample size in the mass spectrometer shows no significant trend with depth (R. Francey, pers. comm., 2000). The flasks containing South Pole firn air were stored for a considerable length of time at sub-ambient pressure, after analysis of other

species including CO_2 and before analysis of $\delta^{13}C$. Contamination during this time **cannot be ruled out** with the available information. It is not clear whether this would have a depth dependence, but it is possible.

In summary, there some possible causes of errors in the firn measurements that cannot be excluded with the available information, but they are not strong enough to use them to choose between the two records.

Other firn $\delta^{13}C$ measurements exist. M. Battle and M. Bender (Princeton Uni., pers. comm.) measured $\delta^{13}C$ in firn air from Siple Dome (Butler et al., 1999). The deepest Siple Dome samples correspond to a CO_2 age somewhere around the time of the CO_2 flattening. If there were problems with collection or measurement of the South Pole firn samples, they may also have occurred for the Siple Dome samples. Firn air was collected at DSSW20K in the 1997/98 summer and $\delta^{13}C$ measured. A different FASD was used, and $\delta^{13}C$ was measured at the same time as CO_2, so this record provides a fairly independent check on the other two. Again, the firn model is required for dating and the diffusion correction. Density but not porosity was measured at DSSW20K. The diffusivity profile as a function of density was calibrated to give the best fit to CO_2, CH_4, SF_6, $\delta^{15}N_2$ and $\Delta^{14}C$ (Figure 3.31). The model gives a good fit to CO_2, SF_6 and CH_4. (CH_4 was modelled with a relative diffusivity of 1.3). Modelled $\delta^{15}N_2$ doesn't agree very well with observations, and the reason for this is not known. The depth where mixing stops agrees with the $\delta^{15}N_2$ measurements, but the fact that all points are below the modelled profile suggests a well mixed region near the surface. The other measurements, however, do not suggest this. The modelled $\Delta^{14}C$ agrees well with the measurements apart from the measurement with highest $\Delta^{14}C$ concentration (at 47 m). By varying the diffusivity profile, it was possible to substantially alter the depth of the $\Delta^{14}C$ pulse in the ice, but only possible to make very minor changes to the amplitude. It was therefore not possible to fit both the highest value and the sides of the peak. It is unlikely that the measurement at the top of the peak is low due to pumping air from a range of depths above and below the peak in the ice. A number of flasks were filled at each depth in the firn, and there is no trend in either CH_4 or CO in the flasks at each depth, which would have been likely if air was pumped from depths significantly above or below the collection depth (D. M. Etheridge, pers. comm., 2000).

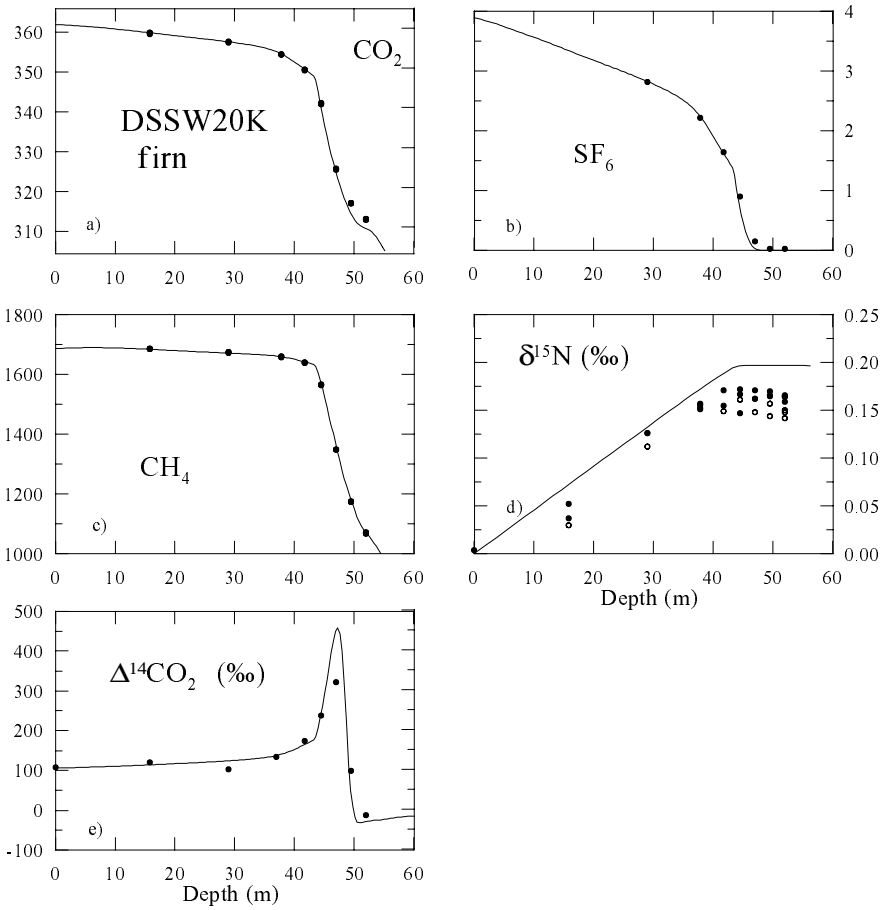

Figure 3.31: Modelled trace gases in the DSSW20K firn. Measurements are unpublished data from CSIRO AR and collaborators (D. Etheridge, pers. comm., 2000). Two $\delta^{15}N_2$ data sets are shown, the solid symbols show measurements of air collected in glass flasks, and the open symbols in metal flasks.

The DSSW20K $\delta^{13}C$ measurements are shown in Figure 3.30b. Two different gravity corrections are applied, one using measurements of $\delta^{15}N_2$ and the other using the modelled $\delta^{15}N_2$ profile. The DSSW20K $\delta^{13}C$ measurements (Figure 3.30b) are lower than the Law Dome $\delta^{13}C$ measurements, although the two lowest DSSW20K samples have slightly high CO_2 values compared with the calculated depth profile and the Law Dome ice core record. The lowest DSSW20K point is around 1940 when dating CO_2 is slightly ambiguous. The fact that the 2 deepest DSSW20K samples have high CO_2 is not consistent with the DE08 model calculations around the 1940s flattening. The RUN3 CO_2 record from Figure 3.16e used in the model for DSSW20K gives an extra dip in concentration just below 50 m, giving

slightly worse fit to deep DSSW20K CO_2 measurements, while the CH_4 fit is excellent. Modelled SF_6 is also too low at the bottom of the firn, although the atmospheric input is not certain because it is extrapolated prior to 1978 (Maiss et al., 1996). In tuning diffusivity, a great number of runs were performed, and none were able to match the change in slope where diffusion stops as well as the CO_2 and SF_6 in the deepest samples.

The DSSW20K measurements have uncertainties of their own, and have not been able to solve the discrepancy between South Pole and Law Dome $\delta^{13}C$ measurements. As plotted in Figure 3.30b, they suggest low $\delta^{13}C$, similar to the South Pole measurements. However if the DSSW20K samples are assigned CO_2 dates by direct comparison of DSSW20K CO_2 with a Law Dome spline, then the $\delta^{13}C$ agree with the Law Dome ice core $\delta^{13}C$.

The $\delta^{13}C$ records presented here are a big step forward from earlier $\delta^{13}C$ records. It has not been possible at this time to explain the discrepancy between the Law Dome and South Pole $\delta^{13}C$ records. The difference between the records gives an indication of the present uncertainties in $\delta^{13}C$ over the 20^{th} century, and the implications of this uncertainty for the carbon cycle will be tested in later chapters. Understanding of the sampling of air and measurement of $\delta^{13}C$ has improved considerably in recent years. Measurement of more samples from Law Dome ice are planned for the future, and they should be able to avoid many of the problems that have been identified by Francey et al. (1999a), and the uncertainties should therefore be reduced. Similarly, precautions could be taken with future firn records to eliminate possible problems, or at least to design tests to check for them.

3.9 Concluding remarks

A model of firn diffusion and bubble trapping has been developed to allow investigation of the characteristics of firn and ice core records compared to their driving atmospheric records. The model quantifies firn smoothing and allows estimation of effective ages for firn and ice core measurements. It is used to correct offsets relative to the atmospheric record, such as the gravitational and diffusion correction for $\delta^{13}C$. The diffusion correction, which corrects for the fact that the heavier isotope diffuses more slowly than the lighter one in the firn, is particularly important for firn and recent ice core $\delta^{13}C$ measurements.

Model calculations focusing on the CO_2 flattening around the 1940s in the DE08 and DE08-2 ice core records were performed to determine how the atmosphere may have changed to leave the measured concentrations in the ice. The model suggests quite strong changes in atmospheric CO_2 to give the observed variations. Measurements of the $\Delta^{14}C$ bomb pulse in firn and ice were compared with model output to try to quantify firn smoothing. The model gives reasonable agreement with the $\Delta^{14}C$ measurements, but there are some uncertainties associated with *in situ* ^{14}C production that need to be resolved before $\Delta^{14}C$ can be used confidently for fine tuning of the model.

A $\delta^{13}C$ firn record from South Pole was constructed by dating firn measurements with the model and applying the gravitational and diffusion corrections. This firn record was then compared with the Law Dome $\delta^{13}C$ ice core record. The South Pole firn record differs from the Law Dome record before about 1970 by an amount that increases with depth (and age of the air) up to a value of about 0.2 ‰. The reasons for this discrepancy are not known, although a number of possible causes were discussed. Quite detailed investigation of another $\delta^{13}C$ firn record, that from DSSW20K, was unable to reduce the uncertainties associated with modelling the site enough for that record to help solve the discrepancy between Law Dome and South Pole.

Analysis of the ice core CO_2 and $\delta^{13}C$ records will benefit greatly from the insight gained in this chapter into the firn processes.

Appendix 3-1 : Model Equations for Mixing Ratio

The diffusion and mass conservation equations are given by

$$J(z) = -D(z)\left[\frac{\partial C}{\partial z} - \frac{MgC}{RT}\right] \tag{A3.1}$$

and

$$\frac{\partial C}{\partial t} = -\frac{\partial}{\partial z}J(z,t) - \lambda C - \frac{1}{f(z)}\frac{\partial f}{\partial z}J(z,t) \tag{A3.2}$$

where $C(z,t)$ is the tracer concentration and the other variables are defined in Section 3.3.1.

Recall that these equations are solved in a moving coordinate system that has velocity $v(z)$ relative to the surface. In this appendix, derivatives are expressed in this moving coordinate system as $\partial/\partial t$ and in the fixed coordinate system as d/dt, and they are related by

$$\frac{\partial}{\partial t} = \frac{d}{dt} + v\frac{d}{dz}$$

As mixing ratios are more commonly measured than concentrations, the diffusion and mass conservation equations are written in terms of mixing ratio, $c(z,t)$, where

$$c(z,t) = C(z,t)/C_{\text{air}} \tag{A3.3}$$

C_{air} is given by the barometric equation

$$C_{\text{air}} = C_0 \exp(\frac{M_{\text{air}}gz}{RT}) \tag{A3.4}$$

and

$$\frac{dC_{\text{air}}}{dz} = \frac{M_{\text{air}}g}{RT}C_{\text{air}} \tag{A3.5}$$

$$\frac{\partial C_{\text{air}}}{\partial t} = v\frac{M_{\text{air}}g}{RT}C_{\text{air}} \tag{A3.6}$$

The derivative of equation (A3.3) is

$$\frac{\partial c}{\partial z} = \left[C_{\text{air}}\frac{\partial C}{\partial z} - C\frac{\partial C_{\text{air}}}{\partial z}\right]/{C_{\text{air}}}^2$$

and by using equation (A3.5) this transforms to

$$\frac{\partial C}{\partial z} = C_{\text{air}}\frac{\partial c}{\partial z} + C\frac{M_{\text{air}}g}{RT} \tag{A3.7}$$

Equations (A3.1) and (A3.7) give

$$J(z) = -D(z)C_{\text{air}}\left[\frac{\partial c}{\partial z} - \frac{(M - M_{\text{air}})gc}{RT}\right] \tag{A3.8}$$

The mixing ratio flux, J_{MR}, is defined as

$$J_{\mathrm{MR}}(z) = -D(z)\left[\frac{\partial c}{\partial z} - \frac{(M - M_{\mathrm{air}})gc}{RT}\right] \tag{A3.9}$$

with

$$J = C_{\mathrm{air}} J_{\mathrm{MR}} \tag{A3.10}$$

If we neglect $\partial C_{\mathrm{air}}/\partial t$, which causes the upward flux of air due to firn compression, we can write

$$\frac{\partial c}{\partial t} = \frac{1}{C_{\mathrm{air}}}\frac{\partial C}{\partial t} \tag{A3.11}$$

This is used in the mass conservation equation, (A3.2), to give

$$\frac{\partial c}{\partial t} = -\frac{1}{C_{\mathrm{air}}}\frac{\partial J}{\partial z} - \lambda c - \frac{1}{f}\frac{\partial f}{\partial z} J_{\mathrm{MR}} \tag{A3.12}$$

Equations (A3.5) and (A3.10) give

$$\frac{\partial J}{\partial z} = C_{\mathrm{air}}\frac{\partial J_{\mathrm{MR}}}{\partial z} + J_{\mathrm{MR}}\frac{M_{\mathrm{air}} g}{RT} C_{\mathrm{air}}$$

This is put into equation (A3.12) to give

$$\frac{\partial c}{\partial t} = -\frac{\partial J_{\mathrm{MR}}}{\partial z} - \lambda c - \frac{1}{f}\frac{\partial f}{\partial z} J_{\mathrm{MR}} - J_{\mathrm{MR}}\frac{M_{\mathrm{air}} g}{RT} \tag{A3.13}$$

Equations (A3.9) and (A3.13) are solved for the mixing ratio, $c(z, t)$, in the firn.